



Norwegian University
of Life Sciences

Master's Thesis 2022 30 ECTS

Faculty of Environmental Sciences and Natural Resource Management

Computational Modelling of Neurons Affected by Transcranial Magnetic Stimulation (TMS)

Jonas Nilsen

Environmental Physics and Renewable Energy

Acknowledgements

A big thank you to my supervisor Torbjørn V. Ness for his help during the making of this thesis. I would also like to thank Gaute T. Einevoll for spreading his enthusiasm for the field of neurological physics.

At home Vibeke has been an indispensable support and through playing disc golf with our friends I've met people face to face and even seen the sun a few times.

Capping it off with our cat Saphie that has been acting as a furry heater in these cold winter days. I even forgive her for nagging about food all the time (don't worry, she isn't exactly ballerina size).

Abstract

Transcranial magnetic stimulation (TMS) is a non-invasive method of stimulation that acts on the brain and is used for both medical and scientific purposes. By accurately simulating what happens inside neurons affected by TMS the results of patient treatment may improve.

To understand what happens during TMS, it is important to have a look at the physics involved. The basic principle is that a time-varying current through a loop of coiled metal wire produces a magnetic field, which induces electric fields. These electric fields then affect neurons. The physics is described in further detail using what appears to be the established consensus. Although there seems to be an established consensus for the basic physics involved, all the processes that takes part in TMS are yet to be fully understood.

Following the path set by others and describing each step in great detail, a model has been created that calculates the current induced inside the neuron, where the neuron is represented as a series of compartments. This induced current is then inserted into compartmental simulation models and the development of the membrane potential of the neuron is simulated for a period of time. The peak current through the coil for these simulations was adjusted to fit the peak magnetic flux density measured for some TMS coils of about 2 Tesla.

The model is made with isolated neurons in mind, but more complex situations could be handled by allowing NEURON to simulate with extracellular potentials and calculating those potentials, although this is outside the scope of this thesis.

The long term goal is to eventually include computational tools for magnetic stimulation of neurons in the toolkit of LFPy.

Sammendrag

Transkraniell magnetisk stimulering (TMS) er en ikke-innvaderende stimuleringsmetode som påvirker hjernen og blir brukt innen medisin og forskning. Ved å simulere hva som skjer på innsiden av nevroner ved bruk av TMS på en nøyaktig måte kan pasientbehandling ved bruk av TMS forbedres.

For å forstå hva som skjer ved TMS er det viktig å undersøke den involverte fysikken. Grunnprinsippet er at det sendes en tidsvarierende strøm gjennom en løkke bestående av en spole i metall som produserer et magnetfelt. Dette magnetfeltet vil indusere elektriske felter og disse elektriske feltene vil påvirke nevroner. Fysikken vil bli beskrevet i detalj ved hjelp av det som virker å være den etablerte konsensusen, men til tross for dette er ikke alle prosessene ved TMS fullt forstått.

Ved å følge i andres fotspor og samtidig forklare hvert steg nøye, har det blitt laget en modell for den induserte strømmen på innsiden av et nevron. Nevronet i denne modellen er delt opp i flere små kamre. Den induserte strømmen blir deretter satt inn i en simuleringsmodell basert på en slik kammermodell og utviklingen av membranpotensialet simuleres over tid. Strømtoppene gjennom spolen under simulering vil bli brukt til å justere modellen slik at den passer med en maksimal magnetisk flukstetthet på ca. 2 Tesla, som er blitt målt for noen spoler under TMS.

Modellen er basert på isolerte nevroner, men mer komplekse situasjoner kan håndteres ved å regne ut de ekstracellulære potensialene. Deretter kan disse simuleres i NEURON, men dette er utenfor denne oppgavens omfang.

Det fremtidige målet er å inkludere beregningsmessige verktøy for magnetisk stimulering av nevroner i LFPy.

Contents

1	Introduction	1
2	Theory	3
2.1	Electric Properties of Neurons	3
2.1.1	RC Circuit	6
2.2	Compartmental Modelling	7
2.3	Generalized Cable Equation for Magnetic Stimulation	9
3	Methods	13
3.1	Simulating a Magnetic Field	13
3.1.1	The Effect of a Magnetic Field on a Neuron	17
3.1.2	Magnetic Flux Density	18
3.2	Compartmental Model	18
3.2.1	Passive Compartmental Model	19
3.3	Table of Default Model Parameters	21
4	Results	23
4.1	The Induced Electric Field	23
4.2	Simulations	30
4.2.1	Comparing Simulations	30
4.2.2	Simulations of Branching Axons	33
4.2.3	Axon Diameter and Membrane Potential	35
4.2.4	Simulation of an Action Potential	37
4.2.5	Simulation of a Complex Neuron	40
4.3	Computational Code	43
5	Discussion	45

Chapter 1

Introduction

The human brain contains about 86 billion neurons and most of these neurons communicate with thousands of other neurons within neural circuits. These neural circuits are parts of bigger neural networks and together with nerves, found in all parts of the body, they are what we call the nervous system. The nervous system handles everything from sensory information and memory to physical movement including heartbeats [19]. As the control center of the nervous system, the complexity of the human brain speaks for itself.

To explore how something as complex as the brain works, information must be gathered through measurements. There are several technologies available that measure different aspects of the activity in the brain and these can be divided into invasive methods (putting foreign objects into the brain) and non-invasive methods (the tools used are kept outside the body). For use on living humans the non-invasive methods offered by brain imaging (i.e. MRI, MEG/EEG, PET, fMRI [5]) is widely used.

In addition to measurements, external sources can be used to stimulate parts of the brain for both medical and scientific purposes. Like the classification used for measurements, external stimuli can also be separated into invasive and non-invasive methods.

Transcranial magnetic stimulation (TMS) is one such non-invasive method of stimulation. It works by sending a time-varying current through a loop of coiled metal wire (formed as one or more circular shapes) placed close to the target area outside the skull. The time-varying current through the coil will then produce a magnetic field which induces electric fields inside the brain. These electric fields, in turn, stimulate areas inside the brain affecting local activity. The most commonly used coil-shapes are either a circle or a figure eight [17] [16].

Even though repetitive TMS (rTMS) has been used in a range of medical

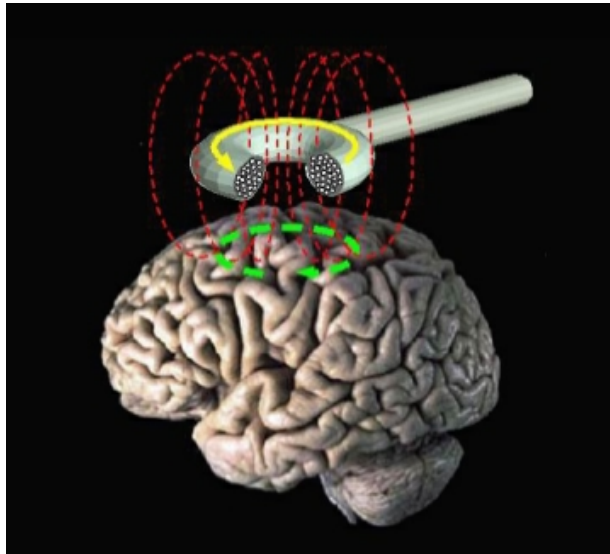


Figure 1.1: Illustration of Transcranial Magnetic Stimulation (TMS). The figure illustrates how a time-varying current passing through a looped coil on the outside the skull produces a magnetic field that induces electric fields inside the brain. Source: Wikimedia Commons, Public Domain [22].

treatments for neurological disorders (like depression, Alzheimer’s disease and movement disorders), the results of the treatment is highly variable. To improve upon this, more detailed computational models of the induced electric fields inside the brain may play an important role [16].

In modern neuroscience the use of computational models have become an important tool to aid in reasoning and to explore how neural behaviour can be connected to measurements from experiments [14]. By using already existing computational tools like LFPy [1] [6] and NEURON [2], alongside a manually created compartmental model using Python [3] syntax, results should be reproducible and transparent.

The goal of this thesis is to gain an understanding of the physics involved in magnetic stimulation of a neuron and create a computational model that can be used to simulate such a scenario based on existing papers and adjust to known TMS setups. A longer term goal is the inclusion of such tools in the LFPy toolkit.

Chapter 2

Theory

This chapter will explain the basic electric properties of a neuron and how a slice of the cell membrane can be represented as a resistor-capacitor (RC) circuit. It will then describe how a series of such circuits can be used in compartmental modelling. At the end of the chapter a generalized cable equation for magnetic stimulation will be derived.

2.1 Electric Properties of Neurons

Neurons consist of a cell body called the soma, dendrites that receive signals from other neurons and axons where signals are sent out to other neurons, as illustrated in Figure 2.1. Both the sending and receiving of signals happen through synapses that connect axons to dendrites.

The cell membrane of a neuron is a vital part of its electric properties with its lipid bilayer and its ion channels controlling the flow of ions through the membrane. The electric potential of a neuron is defined as the potential difference across the cell membrane. The resting membrane potential (or equilibrium potential) is the potential of a neuron when it is in an inactive state. This potential is around -65 mV and indicates that the potential is more negative on the inside of the membrane than on the outside [14]. Neurons can be excitatory, meaning the signals they send will make the receiving neurons more likely to spike (send a signal of their own) or inhibitory, meaning the signals they send will make the receiving neurons less likely to spike [19].

As illustrated in Figure 2.2, the membrane consists of both passive and active parts. The passive parts, the lipid bilayer and the passive ion channels, work on the principle of ion diffusion caused by differences in ion concentrations and electrical drift current caused by potential differences.

2. THEORY

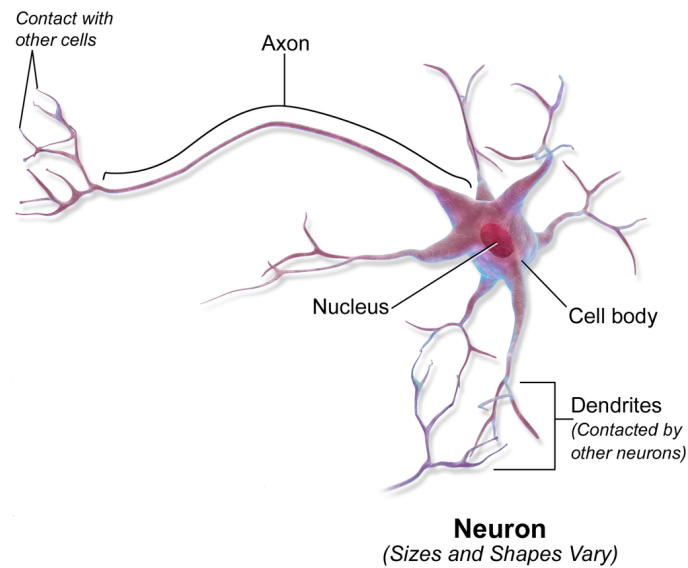


Figure 2.1: Illustration of a neuron. Shows the structure of a neuron, including its axon, dendrites and cell body, usually referred to as the soma. The cell nucleus is inside the soma. Synapses are located at the points where the neuron comes into contact with other cells. Edited, original illustration by Blausen.com staff (2014) [20].

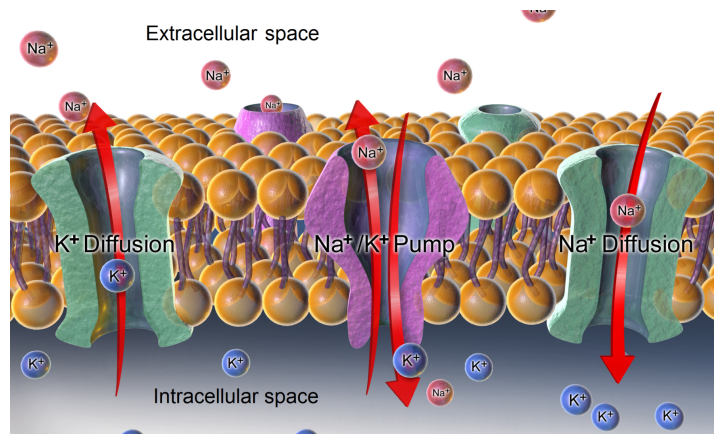


Figure 2.2: Illustration of a patch of membrane from a neuron. Shows the lipid bilayer with its hydrophilic ends (orange spheres) and its hydrophobic ends (purple threads). The additional passageways in purple and green represent the ion channels in the membrane. The purple being active channels (ion pumps) and the green being passive channels (ion diffusion), Illustration by Blausen.com staff (2014) [21].

While the active parts are the active ion channels that typically changes behaviour based on the membrane potential. These active ion channels play an important role when it comes to the creation of an action potential [14].

The action potential is produced when the membrane potential of a neuron reaches a certain threshold. The neuron then sends this action potential as a signal to other neurons which causes those neurons receiving the signal to either increase or decrease their own chance of firing an action potential depending on whether the neuron sending the signal is an excitatory or inhibitory neuron [14].

Axial currents in the intracellular medium (cytoplasm) along a neurite (an axon or a dendrite) will generally obey Ohm's law:

$$I_a = \frac{V_a}{r_a}. \quad (2.1)$$

Here I_a is the axial current [A], V_a is the potential difference along the neurite [V] and r_a is the axial resistance [Ω] [14]. The currents through the cell membrane are not as easily described as the axial currents, because the different parts of the membrane, like ion channels and the membranes ability to accumulate charge, affects its electric properties.

When current passes through the cell membrane it can accumulate charge, acting like a capacitor. The amount of charge is given by:

$$q = c_m V_m. \quad (2.2)$$

Here q is the amount of charge [C], c_m is the membrane capacitance [F] and V_m is the potential difference across the membrane [V] [14]. The current is the same as the rate of change of charge and is given by the derivative of equation (2.2) with respect to time:

$$I_c = \frac{dq}{dt} = c_m \frac{dV_m}{dt}. \quad (2.3)$$

The movement of ions through the cell membrane can be explained by using the Goldman-Hodgkin-Katz (GHK) equations. The GHK current equation can be simplified to a circuit approximation that generally gives useful approximations (for most ions) at membrane potentials that cell membranes are typically exposed to (-100 mV to 50 mV):

$$I_X = g_X(V_m - E_X). \quad (2.4)$$

I_X is the current of ion X passing through the membrane, g_X is the ratio (with units in conductance per unit area) and E_X is the equilibrium potential of ion X . This means that if the membrane potential V_m is equal to the

equilibrium potential E_X , there will be no ion of type X contributing to further membrane polarization or depolarization. This way of representing the ion currents is quasi-ohmic, meaning the linear I-V relation does not pass through the origin. It is useful in its ability to describe the flow of ions, but does not fit well for all ion types. If high detail in specific ion flow is considered important, the quasi-ohmic approximation may not be the best option [14].

2.1.1 RC Circuit

An RC circuit can only be used to describe the passive properties of a neuron, so it is assumed that the membrane acts like a passive core-conductor cable. A more complex model can be used to describe the active properties and the firing of action potentials, like the Hodgkin-Huxley (HH) model [14].

A slice of the membrane can be represented as an electric circuit consisting of a capacitor and several voltage sources in parallel, where each voltage source is connected to a resistor in series. The combination of these voltage sources and resistors represent the ion channels in the membrane and the capacitor represents the membranes ability to accumulate charge [14].

This circuit can be simplified by using Thévenin's theorem, combining several voltage sources and resistances into a single voltage source and a single series resistor. The result of this is an RC circuit like the one in Figure 2.3. By using Kirchhoff's current law (in an electrical circuit, the flow of currents towards and away from a point is equal) together with equations (2.3) and (2.4), an expression for each current can be found [14]:

$$\begin{aligned}
 Ia + I_e &= I_c a + I_i a \\
 I + \frac{I_e}{a} &= I_c + I_i \\
 I_i &= \frac{V_m - E_m}{R_m}
 \end{aligned} \tag{2.5}$$

$$I_c = C_m \frac{dV_m}{dt}. \tag{2.6}$$

Here a is the membrane surface area [m^2], I is the sum of current through the membrane [$\frac{\text{A}}{\text{m}^2}$], I_c is the capacitive current [$\frac{\text{A}}{\text{m}^2}$], I_i is the ionic current [$\frac{\text{A}}{\text{m}^2}$], I_e is the injected current [A], V_m is the membrane potential [V], E_m is the equilibrium potential [V], R_m is the specific membrane resistance [Ωm^2] and C_m is the specific membrane capacitance [$\frac{\text{F}}{\text{m}^2}$].

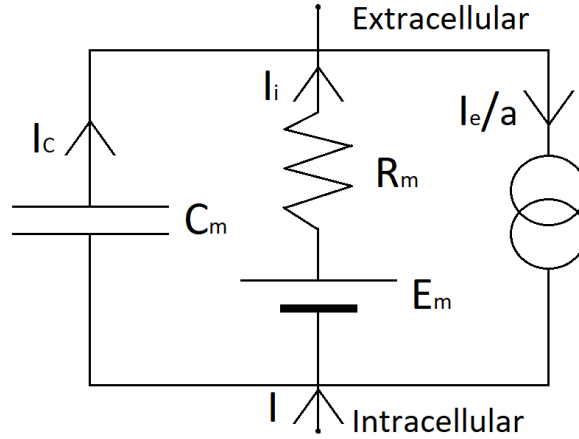


Figure 2.3: RC Circuit for a Patch of Membrane. Shows how a patch of membrane can be represented as an RC circuit and the directions of the currents. The top leads to the extracellular space (outside the membrane) and the bottom leads to the intracellular space (inside the membrane). I is the sum of current through the membrane [$\frac{A}{m^2}$], I_c is the capacitive current [$\frac{A}{m^2}$], I_i is the ionic current [$\frac{A}{m^2}$], I_e is the injected current [A], a is the membrane surface area [m^2], E_m is the equilibrium potential [V], R_m is the specific membrane resistance [Ωm^2] and C_m is the specific membrane capacitance [$\frac{F}{m^2}$].

Assuming the circuit is isolated and combining these two equations gives an ordinary differential equation (ODE) for the membrane potential V_m [14]:

$$C_m \frac{dV_m}{dt} = \frac{V_m - E_m}{R_m} + \frac{I_e}{a}. \quad (2.7)$$

2.2 Compartmental Modelling

A neuron would have to have the same potential everywhere in the cell (isopotential) for the RC circuit to be a good model for its behaviour, but this is generally not the case. A better fit for neuron behaviour is to split it into many smaller cylindrical compartments and consider each compartment as isopotential. Thus, the neuron can be represented as a series of RC circuits (Figure 2.4) for a more detailed model of its behaviour [14].

The cylindrical compartments have length l [m], diameter d [m] and surface area $A_s = \pi dl$ [m^2] (ignoring the top and bottom of the cylinder). The

2. THEORY

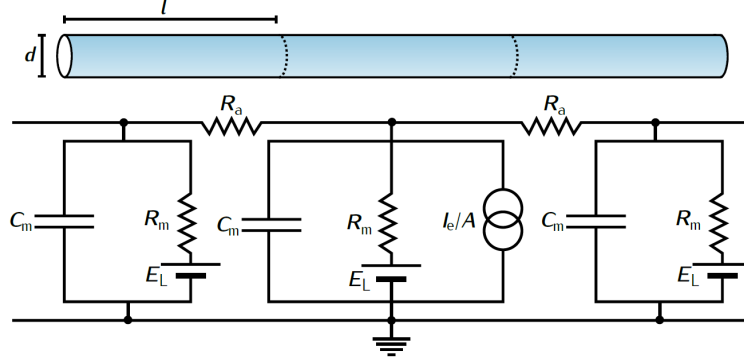


Figure 2.4: Compartmental Model. Illustrates how several connected RC circuits can be used to model a cylindrical cable. Each RC circuit represents a cylinder with diameter d [m], length l [m], surface area $A = \pi dl$ [m²], specific membrane capacitance C_m [$\frac{F}{m^2}$], specific membrane resistance R_m [Ωm^2], equilibrium potential E_L [V] and R_a is the specific axial resistance [Ω] between the compartments/circuits. Figure from *Principles of Computational Modelling in Neuroscience*, page 36, by Sterrat et al. (2011) [14].

surface area of the top and bottom are equal and given by $A_e = \frac{\pi d^2}{4}$ [m²]. Axial resistance is given by $r_a = \frac{R_a l}{A_e} = \frac{4R_a l}{\pi d^2}$ [Ω], where R_a is the specific axial resistance (or axial resistivity) [Ωm]. To simplify the representation of the following equations, it is assumed that all compartments have the same dimensions. The current flowing into compartment j is given by Kirchhoff's current law and Ohm's law [14]:

$$\begin{aligned} I_j A_s &= I_{j-1} + I_{j+1} \\ &= \frac{V_{j+1} - V_j}{r_a} + \frac{V_{j-1} - V_j}{r_a}. \end{aligned} \quad (2.8)$$

From Kirchhoff's current law and equation (2.8) the following equations can be used to describe compartment j :

$$\begin{aligned} I_{c,j} A_s + I_{i,j} A_s &= I_j A_s + I_{e,j} \\ &= \frac{V_{j+1} - V_j}{\frac{4R_a l}{\pi d^2}} + \frac{V_{j-1} - V_j}{\frac{4R_a l}{\pi d^2}} + I_{e,j}. \end{aligned} \quad (2.9)$$

Combining equations (2.5), (2.6) and (2.9) leads to:

$$\pi dl C_m \frac{dV_j}{dt} = \frac{E_m - V_j}{\frac{R_m}{\pi dl}} + \frac{V_{j+1} - V_j}{\frac{4R_a l}{\pi d^2}} + \frac{V_{j-1} - V_j}{\frac{4R_a l}{\pi d^2}} + I_{e,j}. \quad (2.10)$$

Dividing equation (2.10) with $A_s = \pi dl$ gives:

$$\boxed{C_m \frac{dV_j}{dt} = \frac{E_m - V_j}{R_m} + \frac{d}{4R_a} \left(\frac{V_{j+1} - V_j}{l^2} + \frac{V_{j-1} - V_j}{l^2} \right) + \frac{I_{e,j}}{\pi dl}} \quad (2.11)$$

This is the fundamental equation of compartmental modelling and it describes how a series of RC circuits behave when they represent cylindrical compartments [14].

The first and last compartment must be handled in a different way depending on the chosen boundary conditions, where the sealed end condition is a commonly used boundary condition. Under this condition the assumption is that the currents entering or exiting at the ends are negligible because the areas involved are very small, leading to very high resistances. In practise, this is modelled as $V_{start-1} = V_{start}$ for the first compartment and $V_{end} = V_{end+1}$ for the last compartment [14].

2.3 Generalized Cable Equation for Magnetic Stimulation

The models in this thesis make use of the following theory building up to the cable equation for magnetic stimulation, not the equation itself. The final part of the theory has been included for discussional purposes. This section is based on the work of S. Nagarajan and D. M. Durand (1996) [8].

A time-varying magnetic field will induce electric fields in a volume conductor (an axon in this case). Assuming quasi-static conditions [10], [12], [15], these fields can be described using Maxwell's equations [13]:

$$\nabla \cdot \vec{E} = 0 \quad (2.12)$$

$$\nabla \times \vec{E} = -\frac{\partial \vec{B}}{\partial t}. \quad (2.13)$$

The induced electric field \vec{E} has two components; a primary component that is represented as a vector potential \vec{A} and can be considered a direct effect of the applied magnetic field, and a secondary component that is represented as a scalar potential V and can be considered an indirect effect of the applied field due to charge separation on surfaces [13]:

$$\vec{E} = -\frac{\partial \vec{A}}{\partial t} - \nabla V. \quad (2.14)$$

Choosing a gauge (also known as gauge fixing) is a complicated mathematical field, but can in a very simplified comparison be thought of as

2. THEORY

choosing reference points. By choosing the Coulomb gauge, the primary component satisfies both equations below [13]:

$$\nabla \cdot \vec{A} = 0 \quad (2.15)$$

$$\nabla \times \vec{A} = \vec{B}. \quad (2.16)$$

Assuming no external current sources in the intracellular or extracellular regions of the volume conductor. The secondary component then satisfies Laplace's equation [13]:

$$\nabla^2 V = 0. \quad (2.17)$$

Expanding equations (2.15) and (2.17) in cylindrical coordinates [13] and assuming radial symmetry will result in the following equations being independent of the angular derivative [8]:

Primary:

$$\begin{aligned} \nabla \cdot \vec{A} &= \frac{1}{\rho} \frac{\partial}{\partial \rho} (\rho A_\rho) + \frac{1}{\rho^2} \frac{\partial}{\partial \varphi} (\rho A_\varphi) + \frac{\partial A_z}{\partial z} \\ \frac{\partial A_z}{\partial z} &= -\frac{1}{\rho} \frac{\partial}{\partial \rho} (\rho A_\rho). \end{aligned} \quad (2.18)$$

Secondary:

$$\begin{aligned} \nabla^2 V &= \frac{1}{\rho} \frac{\partial}{\partial \rho} \left(\rho \frac{\partial V}{\partial \rho} \right) + \frac{1}{\rho^2} \frac{\partial^2 V}{\partial \varphi^2} + \frac{\partial^2 V}{\partial z^2} \\ \frac{\partial^2 V}{\partial z^2} &= -\frac{1}{\rho} \frac{\partial}{\partial \rho} \left(\rho \frac{\partial V}{\partial \rho} \right). \end{aligned} \quad (2.19)$$

Assume a linear passive core-conductor cable for sub-threshold behaviour of the intracellular volume [14]. Ohm's law in the intracellular region of the volume conductor can then be expressed as:

$$\vec{J}_i = \sigma_i \vec{E}_i. \quad (2.20)$$

Expanding equation (2.20) in cylindrical coordinates gives:

$$I_a = 2\pi\sigma_i \int_0^{b_r} \left(-\frac{\partial A_{z_i}}{\partial z} - \frac{\partial V_i}{\partial z} \right) \rho d\rho. \quad (2.21)$$

This is the same as:

$$r_{a_z} I_a = \vec{E}_i. \quad (2.22)$$

2.3. Generalized Cable Equation for Magnetic Stimulation

For these equations b_r is the radius of the cable [m], I_a is the intracellular axial current [A], r_{a_z} is the axial resistance per unit length [$\frac{\Omega}{\text{m}}$] and \vec{E}_i is the induced electric field in the intracellular region [$\frac{\text{V}}{\text{m}}$]. The derivative of equation (2.21) with respect to z (axial direction):

$$\frac{dI_a}{dz} = 2\pi\sigma_i \int_0^{b_r} \left(-\frac{\partial^2 A_{z_i}}{\partial z \partial t} - \frac{\partial^2 V_i}{\partial z^2} \right) \rho d\rho. \quad (2.23)$$

Assuming azimuthal symmetry (turning an object around an axis, z in this case, does not affect the geometry of the object) and by using equations (2.18) and (2.19), we can rewrite equation (2.23) so that it ends up as an expression for the transmembrane current per unit length:

$$\begin{aligned} \frac{dI_a}{dz} &= 2\pi\sigma_i \int_0^{b_r} \left(\frac{1}{\rho} \frac{\partial^2}{\partial t \partial \rho} (\rho A_\rho) + \frac{1}{\rho} \frac{\partial}{\partial \rho} \left(\rho \frac{\partial V_i}{\partial \rho} \right) \right) \rho d\rho \\ &= 2\pi\sigma_i \left[\left(b_r \frac{\partial A_\rho}{\partial t} + b_r \frac{\partial V_i}{\partial \rho} \right) - \left(0 \frac{\partial A_\rho}{\partial t} + 0 \frac{\partial V_i}{\partial \rho} \right) \right] \\ &= 2\pi\sigma_i b_r \left(\frac{\partial A_\rho}{\partial t} + \frac{\partial V_i}{\partial \rho} \right) \\ &= -i_m. \end{aligned} \quad (2.24)$$

The negative sign comes from the fact that $\nabla \cdot \vec{A}$, the divergence of \vec{A} at a point, is the *outward* flux per unit volume around that point [13].

By linking the membrane current per unit length to a passive membrane, using a capacitance per unit length C_{mz} [$\frac{\text{F}}{\text{m}}$] and a resistance times unit length R_{mz} [Ωm], we get:

$$i_m = C_{mz} \frac{\partial V_m}{\partial t} + \frac{V_m}{R_{mz}}. \quad (2.25)$$

Assuming intracellular potentials vary only along the z axis, equation (2.22) can be expressed as:

$$r_{a_z} I_a = -\frac{\partial A_{z_i}}{\partial t} - \frac{\partial V_i}{\partial z}. \quad (2.26)$$

The transmembrane potential of the secondary component V_m is the difference between the intracellular and extracellular potentials of the secondary component, $V_i - V_e$, caused by charge separation in the volume conductor enveloping the axon. Using this connection ($V_i = V_m + V_e$) equation (2.26) can be rewritten as:

$$r_{a_z} I_a = -\frac{\partial A_{z_i}}{\partial t} - \frac{\partial V_m}{\partial z} - \frac{\partial V_e}{\partial z}. \quad (2.27)$$

2. THEORY

Combining equations (2.24), (2.25) and (2.27) leads to the generalized cable equation:

$$\begin{aligned}
 \frac{dI_i}{dz} &= -i_m \\
 \frac{\partial}{\partial z} \left(\frac{1}{r_{a_z}} \left(\frac{\partial A_{z_i}}{\partial t} - \frac{\partial V_m}{\partial z} - \frac{\partial V_e}{\partial z} \right) \right) &= -C_{mz} \frac{\partial V_m}{\partial t} - \frac{V_m}{R_{m_z}} \\
 \frac{1}{r_{a_z}} \frac{\partial}{\partial z} \left(\frac{\partial A_{z_i}}{\partial t} - \frac{\partial V_e}{\partial z} \right) &= \frac{1}{r_{a_z}} \frac{\partial^2 V_m}{\partial z^2} - C_{mz} \frac{\partial V_m}{\partial t} - \frac{V_m}{R_{m_z}} \\
 \lambda^2 \frac{\partial}{\partial z} \left(\frac{\partial A_{z_i}}{\partial t} - \frac{\partial V_e}{\partial z} \right) &= \lambda^2 \frac{\partial^2 V_m}{\partial z^2} - \tau \frac{\partial V_m}{\partial t} - V_m. \quad (2.28)
 \end{aligned}$$

Here $\lambda^2 = \frac{R_{m_z}}{r_{a_z}}$ is the length constant and $\tau = C_{mz}R_{m_z}$ is the time constant. The left side of this cable equation consists of the contributors to changes in transmembrane potential, also known as driving or forcing functions. The first term, $\frac{\partial}{\partial z} \frac{\partial A_{z_i}}{\partial t}$, is the first spatial derivative of the primary component of the intracellular field. The second term, $\frac{\partial}{\partial z} \frac{\partial V_e}{\partial z}$, is the first spatial derivative of the secondary component of the extracellular field. The membrane thickness is what separates the first term of the the intracellular field and the first term of the extracellular field from being identical, but since this distance is in the scale of nanometers, the changes in the field can be considered insignificant [8]. Because of this, the forcing function can also be expressed as:

$$\begin{aligned}
 f(z) &\cong \lambda^2 \frac{\partial}{\partial z} \left(\frac{\partial A_{z_e}}{\partial t} - \frac{\partial V_e}{\partial z} \right) \\
 &= \lambda^2 \frac{\partial E_{z_e}}{\partial z}. \quad (2.29)
 \end{aligned}$$

Chapter 3

Methods

To simulate how a magnetic field affects a neuron, a model for both the neuron and the electric fields induced by the magnetic field must be in place. These models must then be made in an environment that can handle the simulation. The programming language Python [3] was selected because of its compatibility with LFPy [1] [6] which simplifies interactions with NEURON [2] in addition to its open source distribution. The chapter starts with how the magnetic field is simulated, then looks at how the magnetic field affects a neuron. It follows with how to find the magnetic flux density of the simulated magnetic field and how to model the neuron into cylindrical compartments. At the end of the chapter there will be a table with default model parameters used for simulations.

3.1 Simulating a Magnetic Field

The magnetic field used in TMS comes from a time-varying current passing through a coiled loop. This magnetic field will induce electric fields both inside and outside neurons. The relationship between the magnetic field and the induced electric fields can be described using Maxwell's equations [13]:

$$\nabla \times \vec{E} = -\frac{\partial \vec{B}}{\partial t}. \quad (3.1)$$

The induced electric field \vec{E} in equation (3.1) can, as explained in section 2.3, be expressed as a vector potential and a scalar potential:

$$\vec{E} = -\frac{\partial \vec{A}}{\partial t} - \nabla V. \quad (3.2)$$

3. METHODS

Assuming no charge accumulation, the scalar potential V can be considered insignificant [11], [12], [15]. This leaves the vector potential \vec{A} , which is dependant on the number of loops in the coil N , the geometry of the coil (circle in this case) and the current through the coil I . This can be expressed as:

$$\vec{A} = \frac{\mu IN}{4\pi} \int \frac{\vec{dI}}{R}. \quad (3.3)$$

Here \vec{dI} is a current element, μ is the permeability constant and R is the distance from the current element. The general solution for equation (3.3), given a circular coil, is [9], [15]:

$$\vec{A} = \frac{\mu IN}{\pi k} \left(\frac{r_c}{\rho} \right)^{\frac{1}{2}} \left[K(m) \left(1 - \frac{1}{2}k^2 \right) - E(m) \right] \hat{\theta}. \quad (3.4)$$

The functions $K(m)$ and $E(m)$ are elliptic integrals of the first and second order, while m and k^2 are given by the equation:

$$m = k^2 = \frac{4r_c\rho}{(r_c + \rho)^2 + z^2}. \quad (3.5)$$

Here r_c is the radius of the coil, z is the distance from the center of the coil $(0, 0, 0)$ to the center of the plane parallel to the coil $(0, 0, z)$ and ρ is the distance from the center of the plane $(0, 0, z)$ to the point (x, y, z) . The direction of \vec{A} is given by the unit vector $\hat{\theta}$ which can be found by using the derivative of ρ with respect to θ :

$$\vec{\rho} = \begin{bmatrix} \rho \cos \theta \\ \rho \sin \theta \\ z \end{bmatrix}, \quad \frac{\partial \vec{\rho}}{\partial \theta} = \begin{bmatrix} -\rho \sin \theta \\ \rho \cos \theta \\ 0 \end{bmatrix}$$

$$\left| \frac{\partial \vec{\rho}}{\partial \theta} \right| = \sqrt{(-\rho \sin \theta)^2 + (\rho \cos \theta)^2 + 0^2} = \rho \sqrt{1} = \rho$$

$$\hat{\theta} = \frac{\frac{\partial \vec{\rho}}{\partial \theta}}{\left| \frac{\partial \vec{\rho}}{\partial \theta} \right|} = \begin{bmatrix} -\frac{\rho}{\rho} \sin \theta \\ \frac{\rho}{\rho} \cos \theta \\ 0 \end{bmatrix} = \begin{bmatrix} -\sin \theta \\ \cos \theta \\ 0 \end{bmatrix}. \quad (3.6)$$

The angle θ can be calculated for any point (x, y) in a plane parallel to the coil by using the function $\text{atan2}(y, x)$ included in the math package for Python and $\hat{\theta}$ is then found by using equation (3.6).

Assuming the coil and the volume exposed to the magnetic field does not move in relation to each other, the only value that depends on time will

be the current through the coil. From equation (3.2) we can then find an expression for \vec{E} :

$$\begin{aligned}\vec{E} &\cong -\frac{\partial \vec{A}}{\partial t} \\ &= -\frac{\partial I}{\partial t} \frac{\mu N}{\pi k} \left(\frac{r_c}{\rho}\right)^{\frac{1}{2}} \left[K(m) \left(1 - \frac{1}{2}k^2\right) - E(m) \right] \hat{\theta}.\end{aligned}\quad (3.7)$$

The change in current over time $\frac{\partial I}{\partial t}$ in equation (3.7) causes the magnetic field from the coil to induce an electric field that is oppositely directed from the change in current through the coil. This is the reason for the negative sign in the equation. Splitting the electric field into a spatial function \vec{E}_s (dependant on spatial variables like position and geometry) and a temporal function E_t (dependant on time) results in:

$$\vec{E} = \vec{E}_s E_t. \quad (3.8)$$

The two functions \vec{E}_s and E_t are then given by:

$$\vec{E}_s = -\frac{\mu N}{\pi k} \left(\frac{r_c}{\rho}\right)^{\frac{1}{2}} \left[K(m) \left(1 - \frac{1}{2}k^2\right) - E(m) \right] \hat{\theta} \quad (3.9)$$

$$E_t = \frac{\partial I}{\partial t}. \quad (3.10)$$

The current through the coil can be simulated using an RLC circuit, which is a circuit consisting of a resistor with resistance R , an inductor with inductance L , and a capacitor with capacitance C . In this case the inductor represents the coil. The current in an RLC circuit can either be overdamped (Figure 3.1a), where the current increases to a maximum and then reduces to zero, or underdamped (Figure 3.1b), where the current also increases to a maximum, but instead of reducing directly to zero, it oscillates with less amplitude for each maxima and minima. The two different behaviours can be described with the following equations:

Overdamped:

$$I(t) = V_o C \omega_2 e^{-\omega_1 t} \left(\left(\frac{\omega_1}{\omega_2}\right)^2 - 1 \right) \sinh(\omega_2 t) \quad (3.11)$$

$$\omega_2 = \sqrt{\left(\frac{R_o}{2L_o}\right)^2 - \frac{1}{L_o C}}, \quad \omega_1 = \frac{R_o}{2L_o}. \quad (3.12)$$

3. METHODS

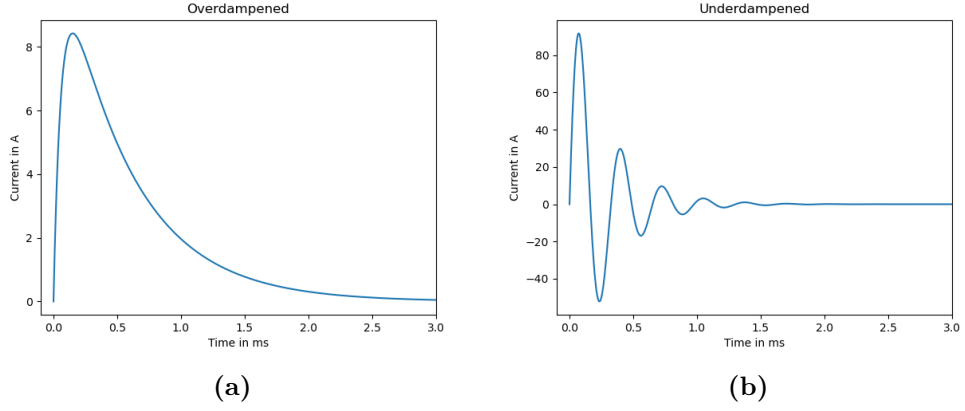


Figure 3.1: RLC circuit behaviour. Example of both an overdamped (a) and an underdamped (b) current in an RLC circuit with $V_0 = 30$ V and $C = 200 \cdot 10^{-6}$ F. For the overdamped case $R_o = 3 \Omega$ and $L_o = 165 \cdot 10^{-6}$ H. For the underdamped case $R_u = 0.09 \Omega$ and $L_u = 13 \cdot 10^{-6}$ H.

Underdamped:

$$I(t) = V_o C \omega_2 e^{-\omega_1 t} \left(\left(\frac{\omega_1}{\omega_2} \right)^2 + 1 \right) \sin(\omega_2 t) \quad (3.13)$$

$$\omega_2 = \sqrt{\frac{1}{L_u C} - \left(\frac{R_u}{2L_u} \right)^2}, \quad \omega_1 = \frac{R_u}{2L_u}. \quad (3.14)$$

The partial derivative of $I(t)$ with respect to time can then be found for both cases using the product rule along with other basic rules of derivation:

Overdamped:

$$\frac{\partial I(t)}{\partial t} = V_o C \omega_2 \left(\left(\frac{\omega_1}{\omega_2} \right)^2 - 1 \right) e^{-\omega_1 t} (\omega_2 \cosh(\omega_2 t) - \omega_1 \sinh(\omega_2 t)). \quad (3.15)$$

Underdamped:

$$\frac{\partial I(t)}{\partial t} = V_o C \omega_2 \left(\left(\frac{\omega_1}{\omega_2} \right)^2 + 1 \right) e^{-\omega_1 t} (\omega_2 \cos(\omega_2 t) - \omega_1 \sin(\omega_2 t)). \quad (3.16)$$

The constants ω_2 and ω_1 are still given by equations (3.12) and (3.14) for the overdamped and underdamped case respectively. The equations (3.15) and (3.16) can then be used to find $\frac{\partial I}{\partial t}$ for any time t and the induced electric field can be calculated using equation (3.8). This can then be implemented in Python syntax to simulate the magnetic field.

The current through the coil is assumed to have an anti-clockwise direction as this corresponds to the positive direction of increasing angles in the standard cylindrical coordinate system. Should the current instead be assumed to move through the coil in a clockwise direction, this can be accounted for by multiplying equations (3.4), (3.7), and (3.9) with (-1) .

3.1.1 The Effect of a Magnetic Field on a Neuron

From equation (2.26) in section 2.3 we have an expression that links the intracellular current with the vector potential of the magnetic field in a situation where there is assumed to be no accumulation of charge in the extracellular volume (an assumption used for calculating the induced electric field in section 3.1). Dividing this by $r_{a_z} [\frac{\Omega}{m}]$ results in:

$$I_a = -\frac{1}{r_{a_z}} \frac{\partial A_{z_i}}{\partial t}. \quad (3.17)$$

The vector potential of the magnetic field in the axial direction $-\frac{\partial A_{z_i}}{\partial t}$ can be expressed as a dot product related to the induced electric field $\vec{E} [\frac{V}{m}]$ by equation (2.14):

$$-\frac{\partial A_{z_i}}{\partial t} = -\frac{\partial \vec{A}}{\partial t} \cdot \hat{a} = \vec{E} \cdot \hat{a}. \quad (3.18)$$

The vector \hat{a} is the unit vector in the axial direction and \vec{E} is the induced electric field. The unit vector \hat{a} is defined as:

$$\hat{a} = \frac{\vec{a}}{|\vec{a}|}. \quad (3.19)$$

Combining equations (3.17), (3.18), (3.19) and the fact that $|\vec{a}|$ is a scalar value:

$$I_a = \frac{1}{r_{a_z}} \frac{\vec{E} \cdot \vec{a}}{|\vec{a}|}. \quad (3.20)$$

Since $|\vec{a}|$ is a distance a [m] in the axial direction that corresponds to the vector \vec{a} [m], then $r_{a_z} a$ is the axial resistance r_a [Ω] for this part of the

3. METHODS

neuron. So equation (3.20) can be written as:

$$I_a = \frac{\vec{E} \cdot \vec{a}}{r_a}. \quad (3.21)$$

By using equations (3.8), (3.9) and (3.10) to calculate the induced electric field \vec{E} , equation (3.21) is an expression for the induced current inside the neuron in the axial direction that can be used to simulate the effect of a magnetic field on a neuron in the situation where there is assumed to be no charge accumulation in the extracellular volume.

3.1.2 Magnetic Flux Density

A setup for TMS can be made using a magnetic flux density B of up to 2 Tesla on a timescale of less than 1 ms [16] [17]. This value can be found for a circular coil with radius r_c and N number of loops, with a current I [A] running counter-clockwise through it, by using the following equation, obtained from using Biot-Savart law on the current through the loop [13]:

$$B = \frac{\mu_0 N I}{2r_c}. \quad (3.22)$$

This magnetic flux density B [T] is found at the center of the coil. Air has a magnetic permeability μ that is very close to the one for vacuum μ_0 , so the difference can be ignored ($\frac{\mu}{\mu_0} \approx 1$). The values for r_c and N are coil specific so the current through the coil I will be the only variable. Equation (3.22) can then be used to find the magnetic flux density B experimentally by running the model with different initial potentials V_0 across the capacitor in the RLC circuit and calculating the current I using equations (3.11) and (3.13).

3.2 Compartmental Model

The basis of a compartmental model is to split something large (a neuron, or part of a neuron in this case) into many smaller pieces (compartments) where the inside of each compartment is treated as being isopotential, as explained in section 2.2. There are several things to consider when creating a compartmental model, such as the geometry of the object to compartmentalize, the placement of the geometry in a coordinate system, changes in potentials and other details depending on the complexity of the model.

3.2.1 Passive Compartmental Model

In a passive model like the one of a core conductor cable represented as a series of RC circuits described in section 2.2, the compartments are usually represented as cylindrical shapes. This is generally a good representation of the shape of a neuron and also the basic form used by NEURON. By making the geometry of the model from input in the form of a .hoc file containing NEURON syntax for creating compartments, comparisons between the manually created compartmental model and NEURON will be simplified. It will also be easier simulate differently shaped structures. An example of syntax in such a .hoc file could be:

```
create axon[1]
axon[0] {
    nseg = 3
    pt3dadd(0, 0, 0, 1)
    pt3dadd(120, 0, 0, 1)
}
```

This would be for an axon with width $d = 1 \mu\text{m}$ and length $l = 120 \mu\text{m}$. The center of the first compartment of the axon is placed in the origin and extends along the x-axis of a Cartesian coordinate system. It consists of one section (axon[0]) that is divided into three segments (compartments). This structure is then used in NEURON through LFPy to create the geometry of the model.

The calculations of the membrane potentials for each compartment will be handled by the fundamental equation for compartmental modelling (2.11). The discrete version used to solve it numerically based on the forward Euler method is:

$$\Delta V_j = \left(\frac{E_m - V_j}{R_m} + \frac{d}{4R_a} \left(\frac{V_{j+1} - V_j}{l^2} + \frac{V_{j-1} - V_j}{l^2} \right) + \frac{I_{e,j}}{\pi dl} \right) \frac{\Delta t}{C_m}. \quad (3.23)$$

Here ΔV_j is the change in potential in compartment j for $\Delta t = t_{i+1} - t_i$. The potential in compartment j for each time step Δt can then be approximated by starting at time $t = 0$ and using:

$$V_{j,t+1} = V_{j,t} + \Delta V_j. \quad (3.24)$$

The induced current in the axial direction of a compartment can be calculated from equation (3.21) in section 3.1.1. Choosing vector \vec{a} to go from the center of compartment j to the center of the next compartment $j + 1$, I_a will then be the induced current [A] and r_a will be the axial

3. METHODS

resistance $[\Omega]$, both between the endpoints of this vector. Using the induced electric field $\vec{E} \left[\frac{\text{V}}{\text{m}} \right]$ at the center of the vector \vec{a} results in:

$$I_{j,j+1} = \frac{\vec{E}_{j,j+1} \cdot \vec{a}_{j,j+1}}{r_a}. \quad (3.25)$$

This equation now calculates the induced current from compartment j to compartment $j + 1$. To make use of this in the model, the induced current must be related to specific compartments. To do this $I_{j,j+1}$ is considered positive in the direction of the vector $\vec{a}_{j,j+1}$ (from j to $j + 1$). A positive current in this direction points out of compartment j and into compartment $j + 1$. The current inserted into compartment j is thus considered negative and equals $-I_{j,j+1}$. The current inserted into compartment j from the same induced current is positive and equals $I_{j,j+1}$. The calculation is repeated for all connections between compartments at all time steps i , resulting in an array I_{input} of the shape $(segments, time)$. This array may then be inserted into equation (3.23) in place of $I_{e,j}$:

$$\Delta V_j = \left(\frac{E_m - V_j}{R_m} + \frac{d}{4R_a} \left(\frac{V_{j+1} - V_j}{l^2} + \frac{V_{j-1} - V_j}{l^2} \right) + \frac{I_{input_{j,i}}}{\pi dl} \right) \frac{\Delta t}{C_m}. \quad (3.26)$$

The output of equation (3.25) when used in the computational model has been chosen as nA $\left(\frac{\text{mV}}{\text{M}\Omega} \right)$ as this is the unit of current used in NEURON.

3.3 Table of Default Model Parameters

For most simulations the parameters in Table 3.1 were used. If different parameters were used in a simulation, it will be specified in the related figure. It may also be specified in the related figure if the parameter is of special interest.

Table 3.1: Default Model Parameters. The table includes the names of the parameters, the symbols used to represent them in the text, their default values for the model and what units these values are given in.

Parameter	Symbol	Value	Units
Membrane Resting Potential	E_m	-70	mV
Specific Membrane Capacitance	C_m	1	$\frac{\mu F}{cm^2}$
Specific Membrane Resistance	R_m	$3 \cdot 10^4$	Ωcm^2
Specific Axial Resistance	R_a	150	Ωcm
Coil Radius	r_c	2	cm
Loops in the Coil	N	30	-
Capacitance for the RLC Circuit	C	200	μF
Resistance for Overdampened RLC Circuit	R_o	3	Ω
Inductance for Overdampened RLC Circuit	L_o	165	μH
Resistance for Underdampened RLC Circuit	R_u	0.09	Ω
Inductance for Underdampened RLC Circuit	L_u	13	μH

Chapter 4

Results

The first part of this chapter will present the simulated induced electric field and attempt to validate it. Afterwards a manually created compartmental model will be compared with a passive NEURON model for identical scenarios. The following part will include simulations with a model for the input current that supports branching, then there will be a simulation that support spiking using the Hodgkin-Huxley model in NEURON. The last simulations will be of a complex neuron structure and at the end of the chapter a link to the computational code can be found.

4.1 The Induced Electric Field

The induced electric field \vec{E} was created from the equations (3.8), (3.9) and (3.10) in section 3.1. The spatial distribution \vec{E}_s of this field is shown in Figures 4.1 and 4.2. Darker colors in these figures represents stronger \vec{E}_s at those points. By looking at the distribution of $|\vec{E}_s|$ in Figure 4.1, it shows that the value of $|\vec{E}_s|$ is largest in the area close to the coil. In the middle of the coil the field is zero.

The equation relating the electric field \vec{E} to the force \vec{F} acting on a stationary particle q in the electric field is given by:

$$\vec{E} = \frac{\vec{F}}{q} \quad , \quad \vec{F} = q\vec{E}. \quad (4.1)$$

A positive charge will experience a force in the positive direction of the electric field [13]. For Figure 4.2 the turquoise color indicates a positive directional vector of \vec{E}_s along the x-axis (a) and y-axis (b), while the brown color indicates a negative directional vector along the same axes. This means that

4. RESULTS

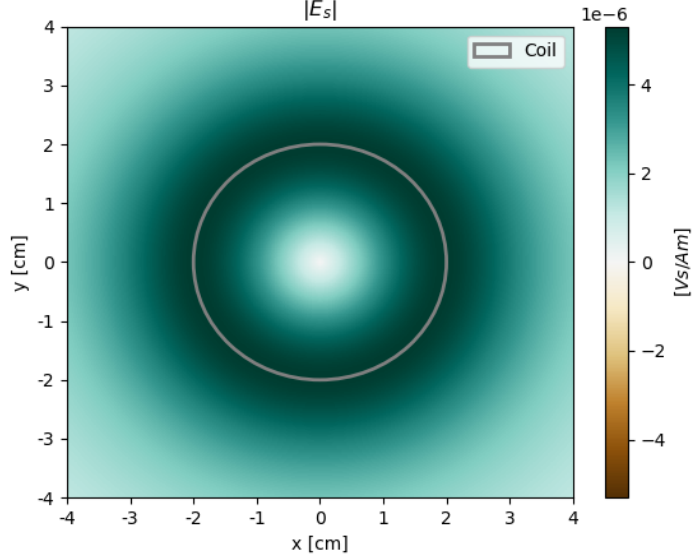
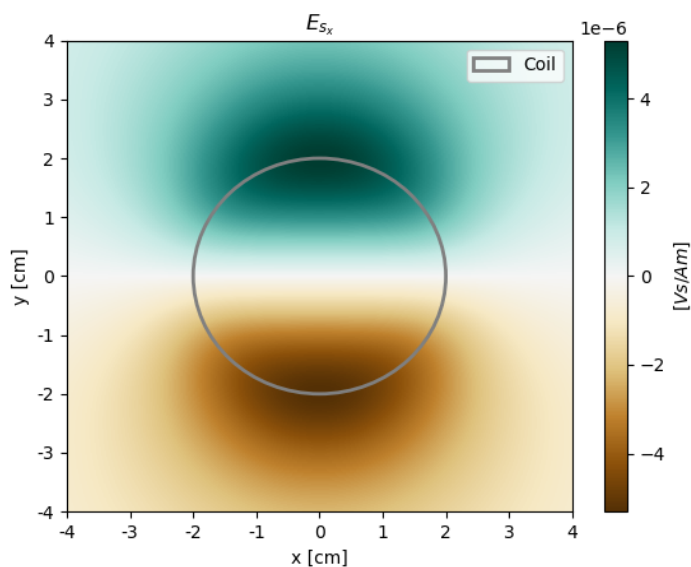


Figure 4.1: Distribution of the spatial field. The figure shows the absolute value of the induced spatial field $|\vec{E}_s|$ [$\frac{V \cdot s}{A \cdot m}$] for the plane $z = 1$ cm below the magnetic coil. The coil has radius = 2 cm and $N = 30$ loops.

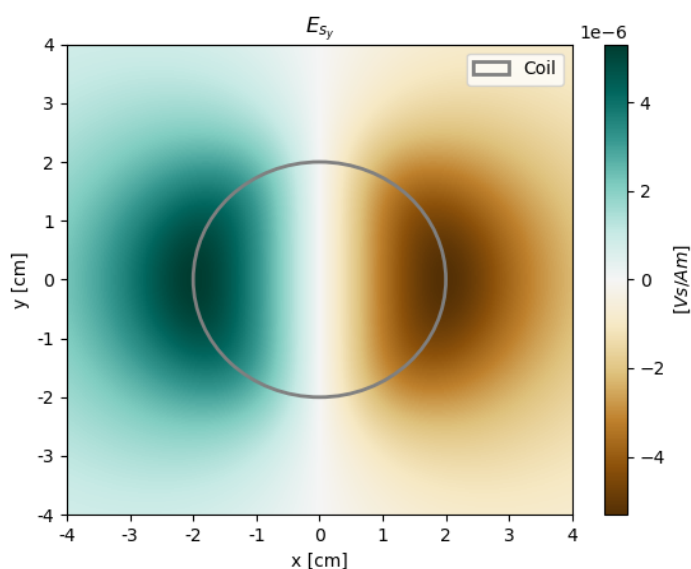
a stationary positive charge q placed in the plane $z = 1$ cm directly underneath the top of the coil (corresponding to the coordinates $(x, y) = (0, 2)$ in Figure 4.1 and 4.2) will experience a force pointing in the positive direction of the x-axis and the same stationary charge q will experience a force pointing in the negative y-direction if placed directly underneath the right side of the coil (corresponding to the coordinates $(x, y) = (2, 0)$ in Figure 4.1 and 4.2).

A circular coil with a time-varying current moving counter-clockwise through it will produce a magnetic field. In a plane directly beneath the coil the magnetic field will induce an electric field and the direction of this induced electric field is expected to point in the opposite direction of the change in current through the coil. Given a positive change in the current in the counter-clockwise direction through the coil, the induced electric field should be directed clockwise at the points directly below the coil. Figure 4.2 indicates that this is true for the simulated induced electric field.

To validate that the manually created compartmental model operates with the expected vector directions given the spatial distributions in Figure 4.2, an axon with three compartments of the same size (S_1, S_2, S_3) can be placed with the center of the middle compartment S_2 at the four points $P_t = (0, 2, -1)$ (top), $P_r = (2, 0, -1)$ (right), $P_b = (0, -2, -1)$ (bottom),



(a)



(b)

Figure 4.2: Distribution of the spatial field in separate directions. Figure (a) shows the x-direction and figure (b) shows the y-direction of the induced spatial field \vec{E}_s [$\frac{\text{V}\cdot\text{s}}{\text{A}\cdot\text{m}}$] for the plane $z = 1$ cm below the magnetic coil. The coil has radius = 2 cm and $N = 30$ loops in both cases.

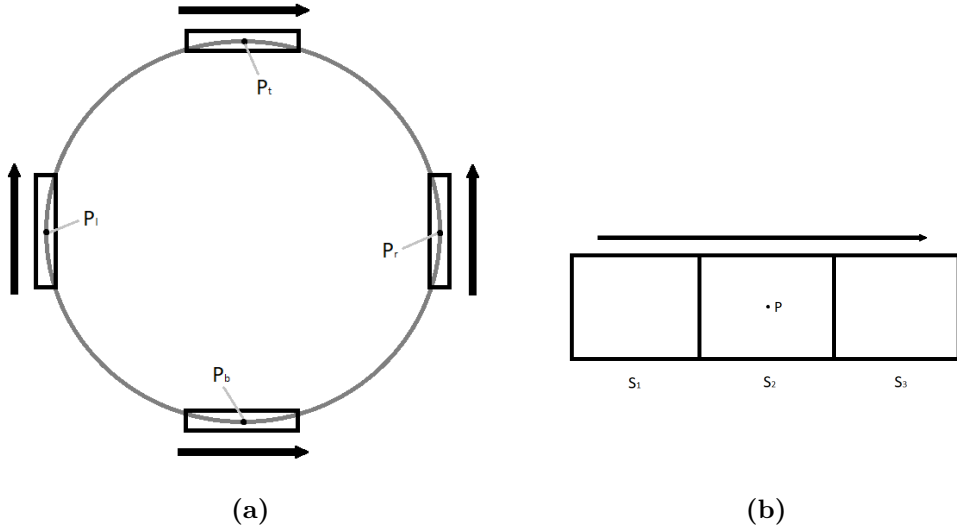


Figure 4.3: Illustration of Axon Placement Relative to Coil. All the axons have width $d = 1 \mu\text{m}$, the length of each compartment is $l = 100 \mu\text{m}$, the coil has radius = 2 cm and the axons are placed in the plane $z = 1 \text{ cm}$ below the coil. The axons are placed in such a way that the arrows in (a) points from compartment S_1 to S_3 as shown in (b). The axons are also placed so that P_t (top), P_r (right), P_b (bottom) and P_l (left) corresponds to the center of S_2 for each axon as shown in (a) and (b). The illustrations are not to scale.

$P_l = (-2, 0, -1)$ (left) as illustrated in Figure 4.3. By placing the axons like this, the expected behaviour for the axons with centers in P_t and P_l is a change in potential from time $t = 0$ that is negative in S_1 and positive in S_3 . For the axons with centers in P_b and P_r the expectation is the opposite, meaning a change in potential from time $t = 0$ that is positive in S_1 and negative in S_3 . The results from simulating the membrane potential of the four axons with the manually created model are shown in Figure 4.4. These results confirm that the output of the manually created compartmental model concur with the expected result.

The induced spatial field \vec{E}_s is only dependant on the structure and placement of the coil. For a specific coil the amplitude of \vec{E} only varies depending on E_t given equation (3.8). Finding an amplitude that is comparable to existing data from TMS experiments was done by calculating the maximum magnetic flux density B of the magnetic field from the coil using equation (3.22), then fitting a current I through the coil, so that $B \approx 2$ Tesla [16] [17]. This was done by keeping the R, L and C components of the RLC circuit constant and varying the starting potential V_0 across the capacitor C at time $t = 0$ in equations (3.11), (3.15) for the overdamp-

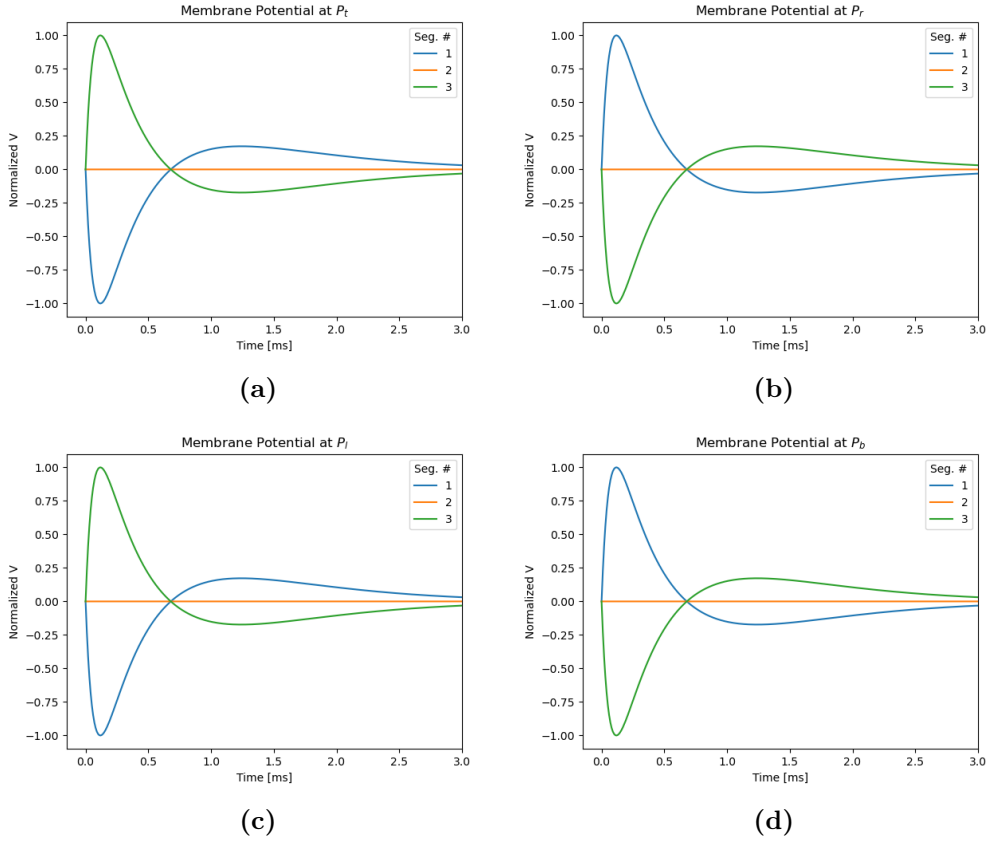
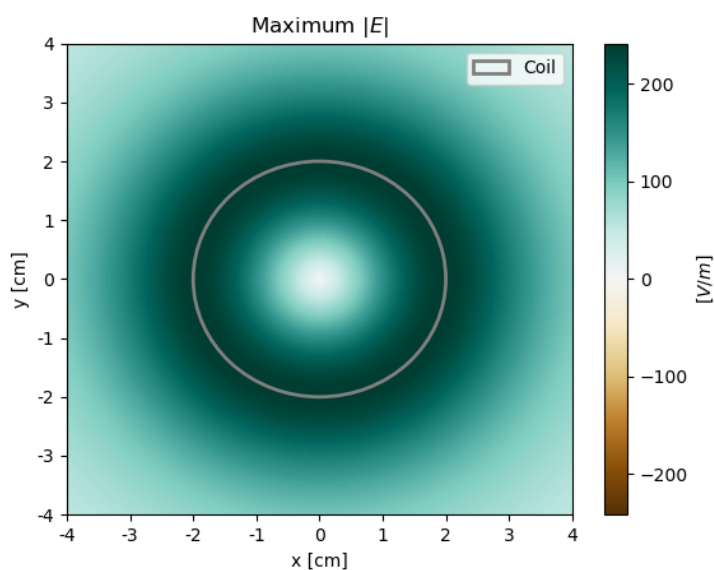


Figure 4.4: Normalized Membrane Potential for Four Axons. The axons are placed as described in Figure 4.3. The blue, orange and green curves represent the first, second and third compartments respectively. All four figures (a-d) were simulated by the manually created compartmental model with the same simulation settings and a duration over 3 ms with a time step of 0.01 ms and the potential was normalized. Resting potential $E_m = 0$ V and an overdamped current was used. The rest of the simulation properties were as given in Table 3.1.

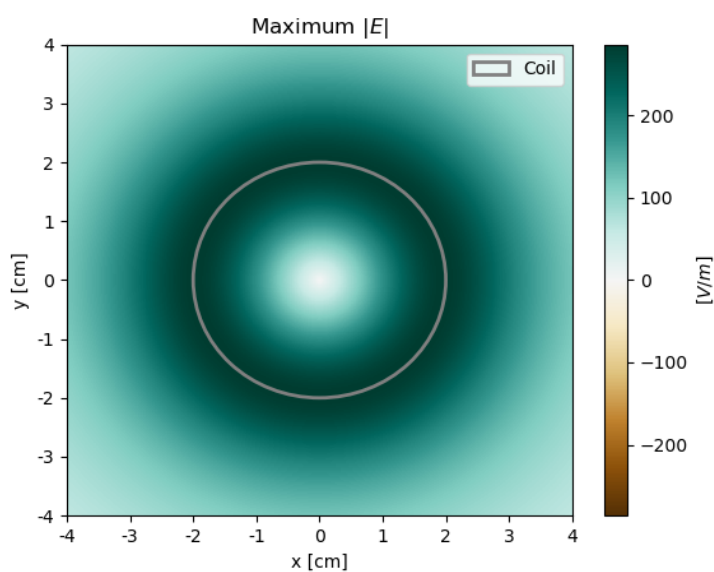
4. RESULTS

ened RLC circuit and equations (3.13), (3.16) for the underdamped RLC circuit.

The distribution of the maximum absolute value of the induced electric field created with $B \approx 2$ T, for both an overdamped and an underdamped current through the coil is shown in Figure 4.5. From this figure the maximum absolute value for the induced electric field $|\vec{E}|$ is in the range of 200 - 300 $\frac{\text{V}}{\text{m}}$.



(a)



(b)

Figure 4.5: Distribution of The Maximum Induced Electric Field. The figure shows the absolute value of the maximum induced electric field $|\vec{E}|$ [$\frac{V}{m}$] for the plane $z = 1$ cm below the magnetic coil. The coil has radius = 2 cm and $N = 30$ loops. For figure (a) the current through the coil is overdamped and the potential across the capacitor is $V_0 = 7500$ V at time $t = 0$ ms. For figure (b) the current through the coil is underdamped and the potential across the capacitor is $V_0 = 700$ V at time $t = 0$ ms. The starting potential difference V_0 was found by using a magnetic flux density $B \approx 2$ T at the center of the coil.

4.2 Simulations

In this section several simulations will be completed and their results shown. The first simulations compare the manually created passive compartmental model with a passive NEURON model. The next part includes more complex structures that allow branching and a look at how the changes in membrane potential scale with axon diameter. The latter parts of this section will include a simulation using the Hodgkin-Huxley model with NEURON to look at spiking behaviour and it will end with simulations of a complex neuron.

4.2.1 Comparing Simulations

The manually created compartmental model only supports passive simulations (no spiking) and single sections, so NEURON was also set to simulate passively and an axon without branches was chosen. A manual compartmental model is more transparent in its handling of potentials and currents than using NEURON, but it is also far less flexible and more prone to errors. To compare the output of the manual compartmental model with the output from NEURON, two axons were placed in different positions relative to the coil and with varying compartment sizes. The axons were then simulated with the same parameters in the manual compartmental model and in NEURON. Input to NEURON through LFPy was done as in the code below:

```
cell_parameters = {
    'morphology': 'simple_axon.hoc',
    'v_init': -70,
    'nsecs_method': None,
    "tstart": 0,
    "tstop": 3,
    "dt": 0.01,
    "Ra": 150,
    "cm": 1,
    "passive": True,
    "passive_parameters": {"g_pas": 1. / 30000,
                           "e_pas": -70},
}
```

The results can be seen in Figures 4.6 and 4.7. There are barely any distinguishable differences between the membrane potential from the manual simulation and the membrane potential from the NEURON simulation.

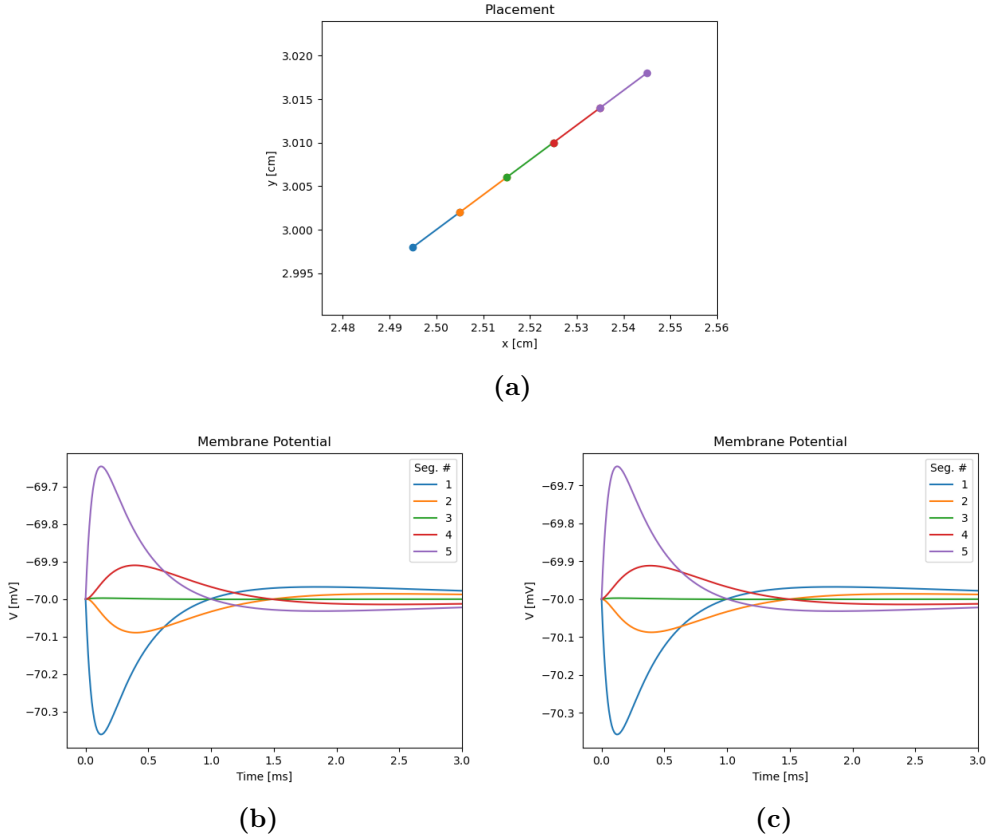


Figure 4.6: Comparing Models by Simulating an Axon (1). The axon was placed with the center of the first compartment in $(x, y) = (2.5, 3)$ cm from the center of the coil $(0, 0)$ in the plane 1 cm below the coil. The axon extends for $500 \mu\text{m}$ along the x -axis and $200 \mu\text{m}$ along the y -axis, and it is $1 \mu\text{m}$ wide. The axon has been divided into five compartments with the same color codes for the three figures. Figure (a) shows the placement of the compartments in the xy -plane. Figure (b) shows the membrane potential for the five compartments from the simulation using the manual compartmental model. Figure (c) shows the membrane potential for the five compartments from the passive NEURON simulation. The simulation was run with an overdamped current through the coil with $V_0 = 7500 \text{ V}$ across the capacitor at time $t = 0 \text{ ms}$ and all other model parameters are presented in Table 3.1.

4. RESULTS

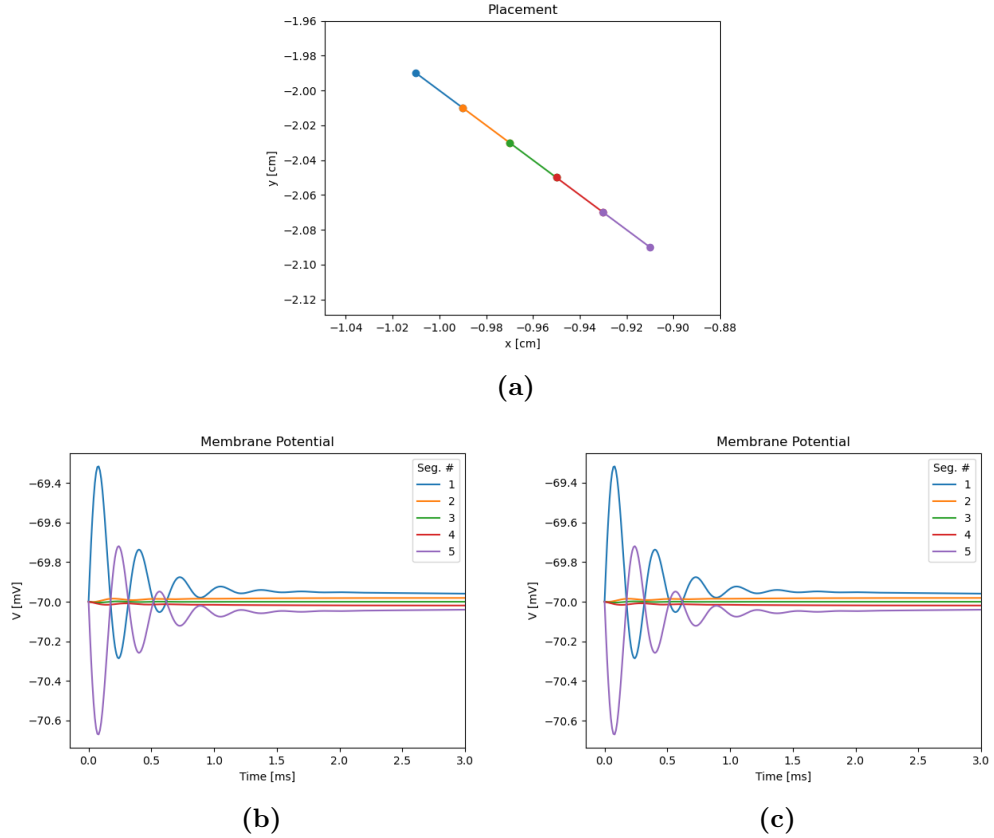


Figure 4.7: Comparing Models by Simulating an Axon (2). The axon was placed with the center of the first compartment in $(x, y) = (-1, -2)$ cm from the center of the coil $(0, 0)$ in the plane 1 cm below the coil. The axon extends for $1000 \mu\text{m}$ along the x-axis and $1000 \mu\text{m}$ in the negative y-direction, and it is $1 \mu\text{m}$ wide. The axon has been divided into five compartments with the same color codes for the three figures. Figure (a) shows the placement of the compartments in the xy-plane. Figure (b) shows the membrane potential for the five compartments from the simulation using the manual compartmental model. Figure (c) shows the membrane potential for the five compartments from the passive NEURON simulation. The simulation was run with an underdamped current through the coil with $V_0 = 700 \text{ V}$ across the capacitor at time $t = 0 \text{ ms}$ and all other model parameters are presented in Table 3.1.

The effect on the membrane potential from the induced electric field can be considered small for both axons (< 1 mV).

4.2.2 Simulations of Branching Axons

NEURON handles neuron structure in the form of sections that extend from point A to point B , then divides those sections into a number of segments (compartments). Sections are then added together by connecting the start of a child section A_c to a point P_{pc} between A_p and B_p on the parent section. The simulations shown so far have been using straight axons that consists of a single section divided into several segments.

To validate that the sectional model for the input current works as expected, it will be compared to the non-sectional model by using three versions of the same axon. In version one the axon consists of one section divided into six segments. In version two the axon consists of two sections, divided into three segments each. In version three the axon consists of six sections that correspond to one segment each. The first version of the axon will be simulated with the non-sectional method, and the other two versions of the axon will be simulated using the sectional model as shown in Figure 4.8.

The results from the test of the sectional model shows that the three different simulations gave the same membrane potentials for the three differently created axons, indicating that the sectional model functions as expected for non-branching axons.

To validate that the sectional model for the input current works as expected when used on a branching axon, a Y-shaped axon is placed with the center of its first compartment in $(x, y) = (0, 2)$ cm in the plane $z = 1$ cm below the coil. The two branching parts will be mirror images of each other across the middle of the axon and they will be pointing along the positive y -axis in the plane (up). Following the results from the tests in section 4.1, the expectation is that the end of the left branch will have a negatively increasing membrane potential from $t = 0$ ms and the end of the right branch will have a positively increasing membrane potential from $t = 0$ ms. This is caused by the induced electric field in the x -direction E_x being positive and much stronger than in the y -direction E_y for this area as shown in Figure 4.2.

Figure 4.9 shows that the expectations for the values of the membrane potentials in the ends of the left and right branch holds, and because $E_y = 0$ at $x = 0$ there is no current inserted from the sectional model into compartments 1 and 2. There is also close to no current inserted into compartment 3, since the effect of the induced electric field \vec{E} between compartment 3

4. RESULTS

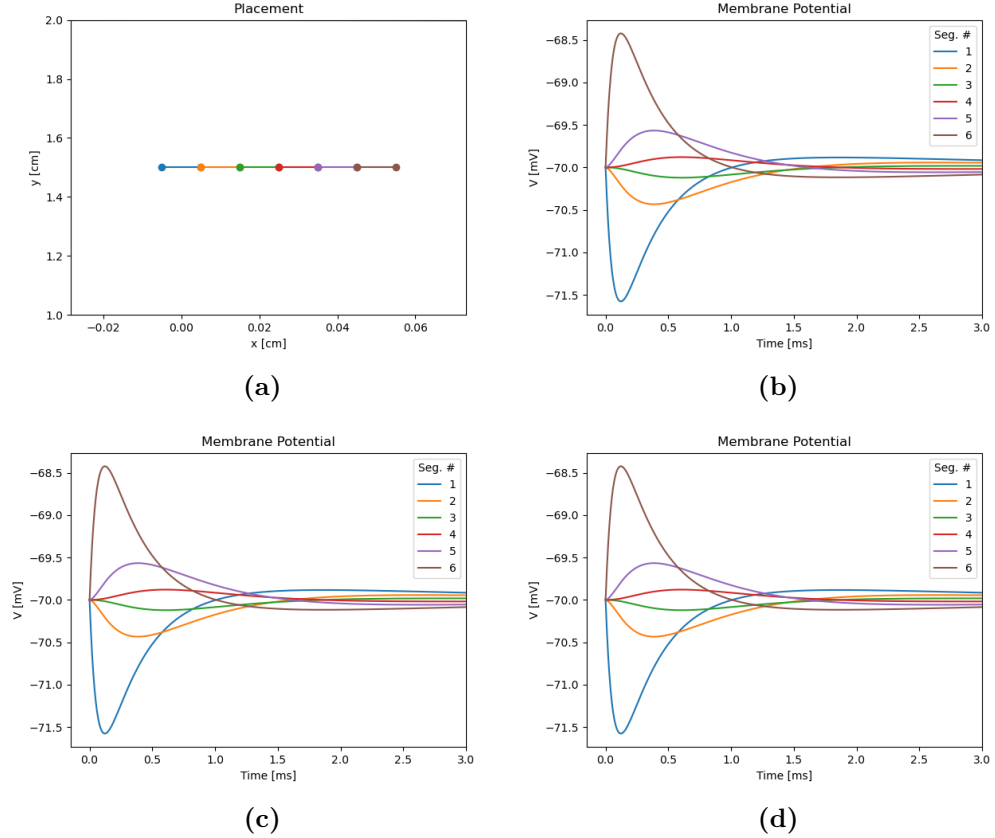


Figure 4.8: Comparing The Sectional Model and The Non-Sectional Model of The Input Current. The axon was placed with the center of the first compartment in $(x, y) = (0, 2)$ cm from the center of the coil $(0, 0)$ in the plane 1 cm below the coil. The axon extends for $600 \mu\text{m}$ along the x-axis and is $1 \mu\text{m}$ wide. The axon has been divided into six compartments in various combinations of sections and segments. Figure (a) shows the placement of the six compartments in the xy-plane. Figure (b) shows the membrane potential for an axon with one section and six segments, simulated with the non-sectional model. Figure (c) shows the membrane potential for an axon with two sections that are divided into three segments each, simulated with the sectional model. Figure (d) shows the membrane potential for an axon with six sections that consist of one segment each, simulated with the sectional model. The simulation was run with an overdamped current through the coil with $V_0 = 7500 \text{ V}$ across the capacitor at time $t = 0 \text{ ms}$ and all other model parameters are presented in Table 3.1. The simulation ran for 3 ms with 0.01 ms time steps in NEURON.

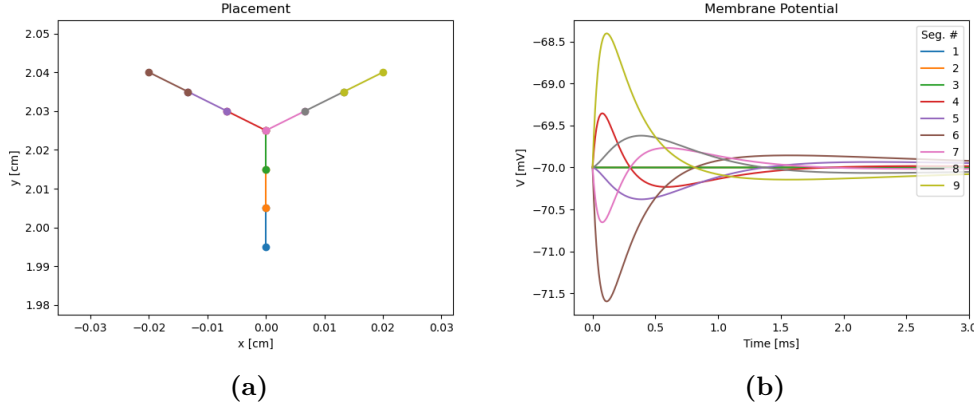


Figure 4.9: Simulation of a Branching Axon. The axon was placed with the center of the first compartment in $(x, y) = (0, 2)$ cm from the center of the coil $(0, 0)$ in the plane 1 cm below the coil. Figure (a) shows the location of the compartments in the three sections of the branching axon. Figure (b) shows the membrane potential during the simulation. The current through the coil is overdamped and the potential across the capacitor is $V_0 = 7500$ V at time $t = 0$ ms and all other model parameters are presented in Table 3.1. The simulation ran for 3 ms with 0.01 ms time steps in NEURON.

and 4 is almost identical to, but oppositely directed from the effect of \vec{E} between compartment 3 and 7 ($E_x \gg E_y$).

4.2.3 Axon Diameter and Membrane Potential

The relationship between the axon diameter and the maximum membrane potential is primarily dictated by the equations (3.25) and (3.26) for the compartmental model. Using these and the definition of $r_a = \frac{R_a l}{A_e} = \frac{4R_a l}{\pi d^2}$ [Ω] from section 2.2, the way the maximum potential scales with the diameter of the compartments can be estimated:

$$\begin{aligned}
 \Delta V_{m_{max}}(d) &\approx \frac{d(\vec{E} \cdot \vec{a})}{4R_a l^2} - \frac{d}{4R_a} \left(\frac{\Delta V_{out}}{l^2} \right) \\
 &\approx \frac{d(\vec{E} \cdot \vec{a}) - d\Delta V_{out}}{4R_a l^2} \\
 &\approx \frac{d(E_{input}) - d\Delta V_{out}}{A_{constant}}.
 \end{aligned} \tag{4.2}$$

Here $d\Delta V_{out}$ is the loss of membrane potential to neighbouring compartments, since the compartment in question will have the highest membrane

4. RESULTS

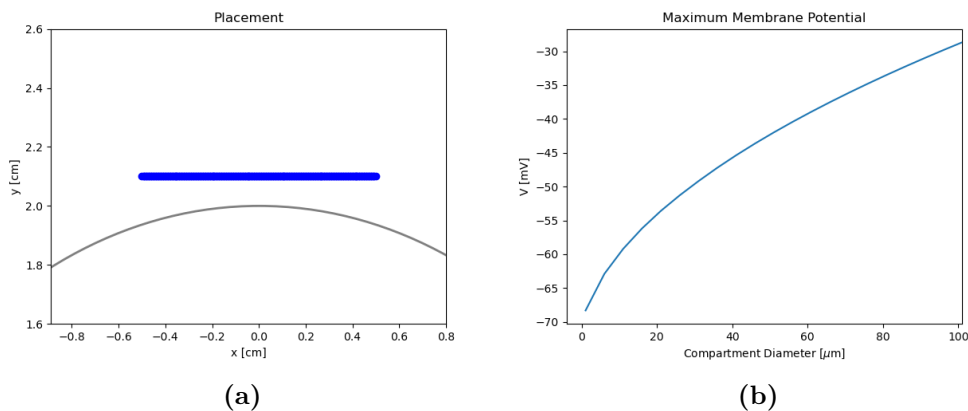


Figure 4.10: Maximum Membrane Potential as a Function of Axon Diameter. The axon was placed with its center in $(x, y) = (0, 2.1)$ cm from the center of the coil $(0, 0)$ in the plane 1 cm below the coil. The axon extends for 1 cm along the x-axis and is divided into 100 compartments, each with length $l = 100 \mu\text{m}$. Figure (a) shows the location of the axon (blue) in relation to the coil (grey). Figure (b) shows the maximum membrane potential as a function of axon diameter. The current through the coil is overdamped and the potential across the capacitor is $V_0 = 7500$ V at time $t = 0$ ms and all other model parameters are presented in Table 3.1. Each simulation ran for 3 ms with 0.01 ms time steps in NEURON.

potential. E_{input} will stay constant while varying the diameter of the compartments. This means that the diameter will increase the change in membrane potential both into and out of the compartment. The higher the maximum potential, the bigger the difference between the compartment with maximum potential and its neighbours. This means that if the diameter d is doubled, the input dE_{input} is doubled and $d\Delta V_{out}$ is more than doubled, but since ΔV_{out} depends on the maximum potential itself, it will not cause the maximum potential to lower with increasing diameters. Because of this, the maximum membrane potential as a function of the diameter of the axon should be a function that increases, but the increase should be less steep for higher diameters as more of the input current is transferred to nearby compartments. The results from the simulations of such a relationship is shown in Figure 4.10 and the maximum membrane potential increases at a lower rate as the diameter of the axon increases.

Figure 4.11 illustrates the same as Figure 4.10, but for a long axon where the accumulation of charge at the ends of the axon is negligible, causing the maximum membrane potential to appear elsewhere. There are slight changes between the simulations, but the difference in maximum membrane

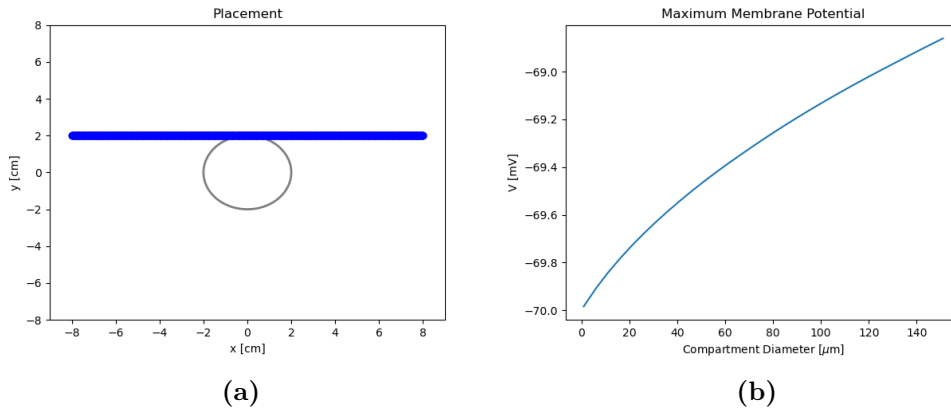


Figure 4.11: Maximum Membrane Potential as a Function of Axon Diameter in a Long Axon. The axon was placed with its center in $(x, y) = (0, 2)$ cm from the center of the coil $(0, 0)$ in the plane 1 cm below the coil. The axon extends for 16 cm along the x-axis and is divided into 500 compartments, each with length $l = 320 \mu\text{m}$. Figure (a) shows the location of the axon (blue) in relation to the coil (grey). Figure (b) shows the maximum membrane potential as a function of axon diameter. The current through the coil is overdamped and the potential across the capacitor is $V_0 = 7500 \text{ V}$ at time $t = 0 \text{ ms}$ and all other model parameters are presented in Table 3.1. Each simulation ran for 3 ms with 0.01 ms time steps in NEURON.

potentials are significant between the two cases.

4.2.4 Simulation of an Action Potential

A passive model can give useful data about membrane potentials, but will not have the ability to create an action potential (spike). To simulate such an action potential the Hodgkin-Huxley model (HH-model) can be used. It is also readily available through NEURON.

The original HH-model is based on a squid giant axon, but it can be used for other axons by fitting certain parameters to experimental data. It works by handling the different types of ion channels separately. It has some new parameters compared to the passive compartmental model used so far, including the equilibrium potential for each ion type E_{ion} and the probability of an ion type passing through an ion channel (ion conductance) \bar{g}_{ion} . There is also an additional grouping of currents referred to as the leak current l_c [14].

Making the HH-model initiate an action potential requires the membrane potential to pass a certain threshold. The settings used for the cal-

4. RESULTS

culuation of the induced electric field so far will not cause the membrane potential to pass this threshold in a very long straight axon. To bypass this the starting potential V_0 across the capacitor in the RLC circuit must be increased by a large amount in addition to the changes in settings caused by using the HH-model. By using a very long axon (16 cm) that reaches far outside the the area where the induced electric field is the strongest, the action potential will not be generated at one of the ends of the axon.

The simulation using the HH-model is visualized in Figure 4.12. This shows that the axon placed along the x-axis with its center at $(x, y) = (0, 2)$ cm from the center of the coil experienced the largest positive membrane polarization at around $x = 1.8$ cm, since this is where the action potential originated. The figure illustrates how this action potential propagates along the axon to the left and right of its source.

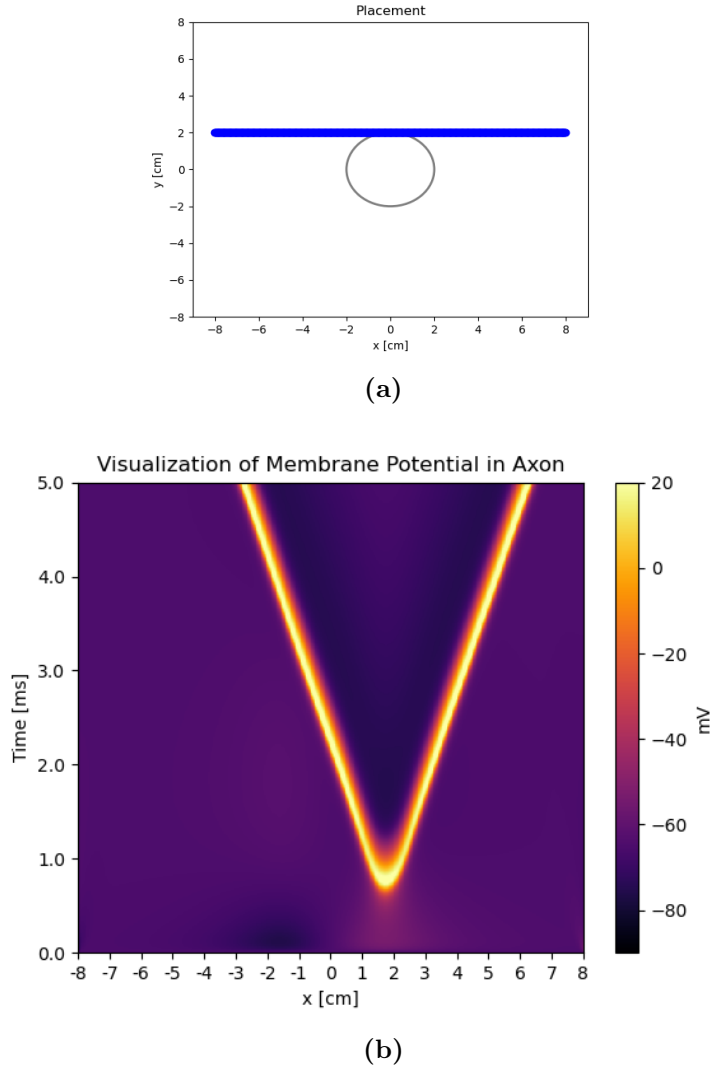


Figure 4.12: Visualization of an Action Potential Using the Hodgkin-Huxley model. The axon was placed with its center in $(x, y) = (0, 2)$ cm from the center of the coil $(0, 0)$ in the plane 1 cm below the coil. The axon extends for 16 cm along the x-axis and is divided into 500 compartments, each with length $l = 320 \mu\text{m}$ and width $d = 100 \mu\text{m}$. Figure (a) shows the location of the axon (blue) in relation to the coil (grey). Figure (b) is the visualization of the membrane potential of a very long axon, each compartment is placed along the x-axis and its membrane potential is shown for each time step. The current through the coil is overdamped and the potential across the capacitor is $V_0 = 30000$ V at time $t = 0$ ms, which gives a maximum magnetic flux density of about 8 Tesla at the center of the coil. The simulation ran for 5 ms with 0.01 ms time steps using the HH-model in NEURON. HH-model parameters: $R_a = 35.4 \Omega\text{cm}$, $C_m = 1 \frac{\text{F}}{\text{cm}^2}$, $\bar{g}_{na} = 0.12 \frac{\text{S}}{\text{cm}^2}$, $\bar{g}_k = 0.036 \frac{\text{S}}{\text{cm}^2}$, $\bar{g}_{lc} = 0.0003 \frac{\text{S}}{\text{cm}^2}$, $E_{na} = 50$ V, $E_k = -77$ V, $E_{lc} = -54.387$ V and the initial membrane potential was set to -65 V.

4.2.5 Simulation of a Complex Neuron

All simulations so far have targeted structures that only extend along the x- and y-axes in a plane below the coil. To simulate a complex neuron, the structure has to extend along the z-axis as well. Assuming the z-axis is perpendicular to the surface of the tissue (brain), the z-component of the electric field induced by the magnetic field is zero according to Tofts 1990 [15]. This means that the only contribution from the z-axis is its effect on the induced electric field in equation (3.5), reducing the effect of the field with increasing distance from the coil.

The complex cell structure (morphology) chosen is the Hay-Cell ("cell #1") with parameters from Table 3 in Hay et al. (2011) [7]. This cell was chosen because code for its implementation with LFPy already exists. The results of the simulations of the neuron is shown in Figures 4.13 and 4.14. The compartments chosen for illustrating the membrane potential is the soma and a compartment about 500 μm away from the soma along the y-axis.

The effect of the magnetic field on the membrane potential of the two compartments is small, but not insignificant, at approximately 2 mV. The soma is also depolarized in the first simulation in Figure 4.13 and polarized in the second simulation in Figure 4.14, indicating that different placements and orientations of the cell may lead to increased or decreased chances of firing an action potential.

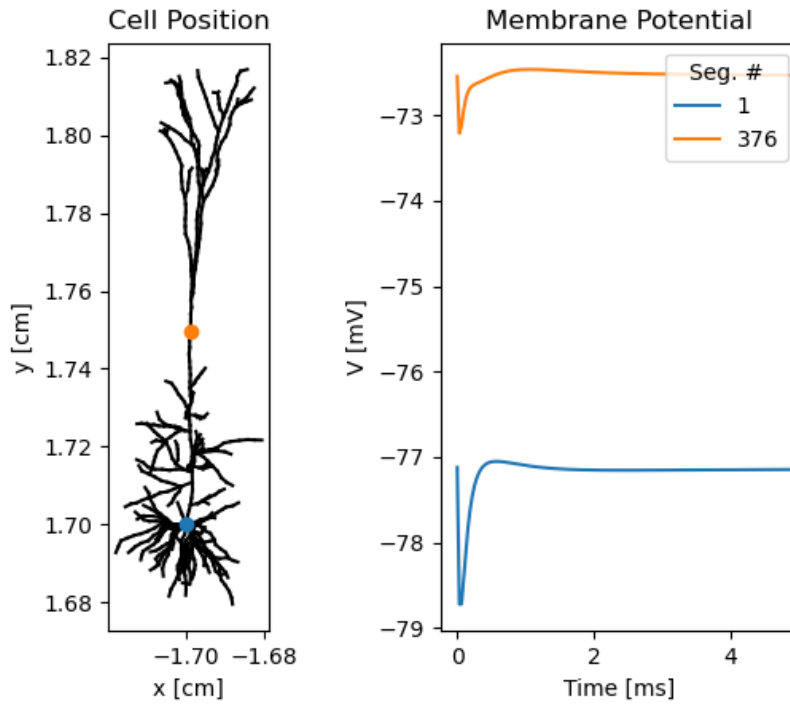


Figure 4.13: Simulation of a Complex Neuron Represented by The Hay-Cell (1). The Hay-Cell has been placed with the center of its soma-compartment at $(x, y) = (-1.7, 1.7)$ cm from the center of the coil. The left figure shows the position of the cell and the two colored compartments represent the soma (blue) and a compartment (orange) in the axon about $500 \mu\text{m}$ away from the soma along the y -axis. The right figure shows the development of the membrane potential for these two compartments. The current through the coil is overdamped and the potential across the capacitor is $V_0 = 7500 \text{ V}$ at time $t = 0$ ms. Each simulation ran for 5 ms with 2^{-5} ms time steps in NEURON. Complex neuron based on "cell #1" with parameters from Table 3 in Hay et al. (2011) [7].

4. RESULTS

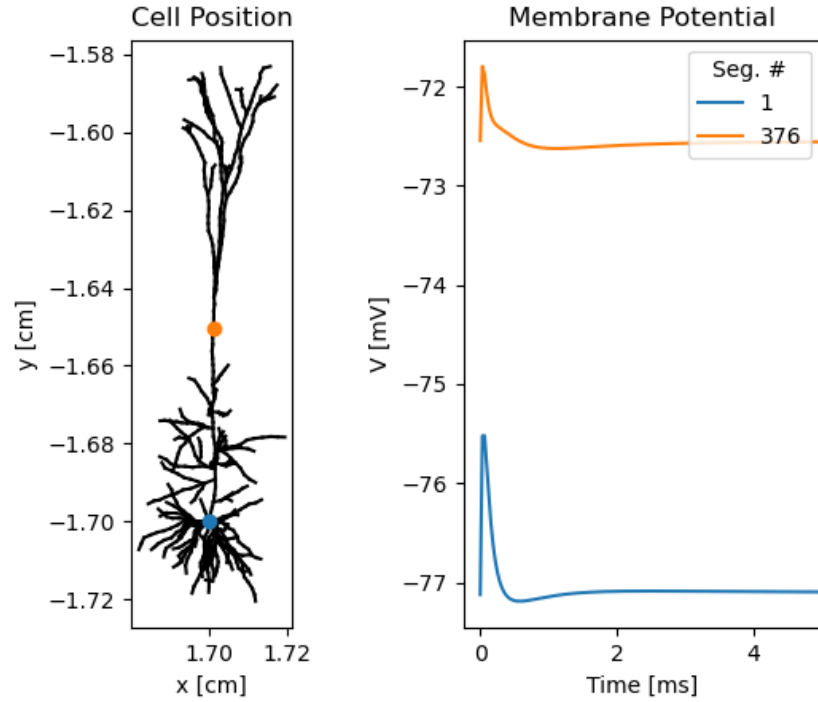


Figure 4.14: Simulation of a Complex Neuron Represented by The Hay-Cell (2). The Hay-Cell has been placed with the center of its soma-compartment at $(x, y) = (1.7, -1.7)$ cm from the center of the coil. The left figure shows the position of the cell and the two colorized compartments represent the soma (blue) and a compartment (orange) in the axon about $500 \mu\text{m}$ away from the soma along the y-axis. The right figure shows the development of the membrane potential for these two compartments. The current through the coil is overdamped and the potential across the capacitor is $V_0 = 7500$ V at time $t = 0$ ms. Each simulation ran for 5 ms with 2^{-5} ms time steps in NEURON. Complex neuron based on "cell #1" with parameters from Table 3 in Hay et al. (2011) [7].

4.3 Computational Code

The code used for these results requires Python 3, NEURON and LFPy. It does not support systems running Windows, but this can be solved by using a virtual environment.

All the code is available through Git-Hub:
'<https://github.com/Jonasnil/Masters.git>'

Chapter 5

Discussion

Magnetic Field

The simulations utilized a magnetic field from equation (3.4) used by Pashut et al. 2011 [9] and the parameters of the RLC circuit in Table 3.1 are the same as the ones used by Pashut et al. 2011 [9] and almost the same as the ones used by Roth et al. 1990 [12]. The magnitude of the magnetic field was decided from a peak magnetic flux density of about 2 Tesla during TMS [16], [17].

The potential across the capacitor in the RLC circuit at the beginning of a simulation (V_0) that was needed to reach a magnetic flux density of about 2 Tesla ended up being 7500 V for the overdamped circuit and 700 V for the underdamped circuit. By using this V_0 the maximum absolute value of the induced electric field is in the range of 200 - 300 $\frac{\text{V}}{\text{m}}$ for both the overdamped and the underdamped current through the coil as shown in Figure 4.5. This is on the same scale as in experimental recordings at around 100 $\frac{\text{V}}{\text{m}}$ maximum induced electric field on the cortical surface [16].

This initial potential $V_0 = 7500$ V was a lot bigger than the ones used by Roth et al. 1990 [12] and Pashut et al. 2011 [9] ($V_0 = 30 - 36$ V), but the reason for their choice of V_0 was not made transparent. In general, transparency for calculations and parameter choices seemed low for magnetic stimulation of neurons, making direct comparisons difficult in many cases.

Comparing the magnetic field from Figures 4.1 and 4.2 to the ones from Pashut et al. 2011 [9], shows that they are on the same scale, but E_x and E_y is oppositely directed. Since the positive direction of the current through the coil is not specified in their paper it is difficult to find the reason for the difference, but the testing done for the magnetic field in Figure 4.4 indicates that the x- and y-distributions in Figure 4.2 are as expected.

5. DISCUSSION

An assumption for the calculation of the magnetic field that was used, is that there is no charge accumulation in the extracellular medium. This is only valid in the case of an isolated neuron, so the current inserted into the neuron by using equation (3.21) only accounts for the magnetic field from the primary component $-\frac{\partial \vec{A}}{\partial t}$, from equation (2.14), affecting the inside of the neuron. To make the model account for the secondary component of the magnetic field $-\nabla V$, from equation (2.14), the handling of the external field would have to be included.

As the generalized cable equation for magnetic stimulation (2.28) shows, the driving forces behind the changes in membrane potential V_m is the primary part of the magnetic field in the intracellular region $\frac{\partial \vec{A}_{z_i}}{\partial t}$ and the secondary part of the magnetic field in the extracellular region $\frac{\partial V_e}{\partial z}$. By separating the terms in equation (2.26) the input current that the model handles in equation (3.21) corresponds to the input from the first term $-\frac{\partial \vec{A}}{\partial t}$, and the extra current from the other term $\frac{\partial V_e}{\partial z}$ can be handled separately through equation (2.27):

$$\vec{E} = \vec{E}_{prim} + E_{sec} \quad (5.1)$$

$$\vec{E}_{prim} = r_{iz} I_{ap} = -\frac{\partial \vec{A}_{z_i}}{\partial t} \quad (5.2)$$

$$E_{sec} = r_{iz} I_{as} = -\frac{\partial V_i}{\partial z} = -\frac{\partial V_m}{\partial z} - \frac{\partial V_e}{\partial z}. \quad (5.3)$$

From these three equations, the existing model for the intracellular field, equation 5.2, should be compatible with using the extracellular scalar field from the secondary component to account for the accumulation of charge in the extracellular medium using equation (5.3). This is because it should be possible to calculate the two terms separately. The external field can then be inserted into NEURON and its calculations for external potentials can be used. Inserting external potentials in NEURON is a relatively simple process, so the challenge will be finding the correct extracellular potentials for all compartments.

Another approach could be to handle all the input to a compartment from the magnetic field through the extracellular calculations in NEURON, as done by Wang et al. 2018 [18] and Aberra et al. 2019 [4]. This is possible by using the connection that leads to equation (2.29), which states that the distance separating the intracellular and extracellular vector potentials from the primary component in the axial direction is on the scale of nanometers, and the change in the vector potential over this distance can be considered insignificant.

Simulations

The simulations in the first part of Chapter 4 is focused on justifying certain aspects of the model, like the directions of the induced electric field and the membrane potential in axons placed at certain locations (Figure 4.4) as well as the symmetry of a branching axon (Figure 4.9). These results indicate that the model works as intended, but are not a guarantee for correct calculations. All input data and calculated values have been shown, or an explanation has been attempted, so comparisons can easily be made and most aspects of the models are transparent.

With the maximum absolute value of the induced electric field ($|\vec{E}_{max}| < 300 \frac{\text{V}}{\text{m}}$) being on the same scale as observed on the scalp during TMS ($\approx 100 \frac{\text{V}}{\text{m}}$) [16], the data from simulations should, in theory, have useful results for isolated neurons.

The effect of the induced electric field on the axons in Figures 4.10 and 4.11 indicates that areas inside neurons where the movement of currents are limited or obstructed (resulting in dipoles) will experience a larger change in membrane potentials than areas where currents can move more freely. Even in the ends of axons, the changes in membrane potential can still be considered small ($< 3 \text{ mV}$) for axons with diameters of $1 \mu\text{m}$ that extends for less than $1000 \mu\text{m}$ as seen in Figures 4.6, 4.7, 4.8 and 4.9. The changes in membrane potential for a complex neuron is on the same scale as shown in Figures 4.13 and 4.14, but small changes in membrane potentials can still cause action potentials that would not have been initiated otherwise [14].

It is worth noting that the simulations are for only one pulse of TMS and does not represent the complete treatment used on patients [16].

Challenges

During the comparisons between papers and the creation of both the manual compartmental model and the model for the input current from the induced electric field, it was difficult finding all the correct units used for the different variables. As an example, in this thesis resistance is used in four different forms, including the specific resistances, and all of them are related to units of length or area in separate ways. This is also the reason why units are shown alongside most variables in this thesis.

As already discussed, the lack of transparency for calculations and parameters seemed low in general and this made it difficult to do direct comparisons with papers using the same methods.

The author's knowledge of communicating with NEURON directly was not extensive before this thesis. This resulted in some of the solutions used

and steps taken in the code being redundant or having simpler alternatives. This has not affected the functionality of the models, but the code could have been made less cluttered. There was also the usual issues involved in creating computational code, but the bugs were all hopefully found and fixed.

Magnetic Stimulation and LFPy

The long term goal is to eventually include computational tools for magnetic stimulation of neurons in the toolkit of LFPy, but in addition to working correctly, the implementation itself should make sense and be adaptable.

The current code made for this thesis is not the best solution as it is too hardcoded with one specific coil setup in mind. A better way of implementing it into LFPy would be to separate the calculations of the induced electric field from the calculation of the input current. This way it will be easier to do simulations for different coil shapes and also leaves the option of supplying the field directly from experimental data recordings.

The next part would then be to calculate the input current. This could be handled in different ways as described in the discussion about the magnetic field, but implementing several solutions should not be an issue.

A simplified example of using such an implementation could then look like:

```
# Creating the neuron shape using already existing syntax:
cell = LFPy.Cell(**cell_parameters)

# Calculating the required field for a specific coil:
cell.coil_circle(**coil_parameters)

# Or by supplying the field as data:
cell.supplied_field_data(data_file)

# Then using the previous field to get input currents and
# insert into NEURON as done in this thesis:
cell.calc_input_currents()

# Or using the field to calculate external potentials:
cell.calc_ext_field()

# Then simulate using NEURON as you would normally do:
cell.simulate()
```

This example code is primarily for illustrating the steps as an actual implementation would most likely require less user interaction and be handled through one function call between the creation of the cell and the simulation of it.

Bibliography

- [1] LFPy v2.2.4, online documentation. Last accessed 12.2022. '<https://lfpypy.readthedocs.io/en/latest/>'.
- [2] NEURON v8.0.0, online documentation. Last accessed 12.2022. '<https://neuron.yale.edu/neuron/docs>'.
- [3] Python v3.9.10, online documentation. Last accessed 12.2022. '<https://docs.python.org/3/>'.
- [4] Aman S. Aberra, Boshuo Wang, Warren M. Grill, Angel V. Peterchev. Simulation of Transcranial Magnetic Stimulation in Head Model with Morphologically-Realistic Cortical Neurons. *Brain Stimulation*. 13(1), 175-189, January 2020. '<https://doi.org/10.1016/j.brs.2019.10.002>'.
- [5] Gaute T. Einevoll. Lecture notes from the course Computational Neuroscience at NMBU, 2022.
- [6] Espen Hagen, Solveig Næss, Torbjørn V. Ness, Gaute T. Einevoll. Multimodal Modeling of Neural Network Activity: Computing LFP, ECoG, EEG, and MEG Signals With LFPy 2.0. *Front. Neuroinform.*, 12:92. '<https://doi.org/10.3389/fninf.2018.00092>'.
- [7] Etay Hay, Sean Hill, Felix Schuermann, Henry Markram, Idan Segev. Models of Neocortical Layer 5b Pyramidal Cells Capturing a Wide Range of Dendritic and Perisomatic Active Properties. *PLoS Computational Biology* 7(7), 1–18, July 2011.
- [8] Srikantan S. Nagarajan, Dominique M. Durand. A Generalized Cable Equation for Magnetic Stimulation of Axons. *IEEE Transactions on Biomedical Engineering*. 43(3), March 1996.
- [9] Tamar Pashut, Shuki Wolfus, Alex Friedman, Michal Lavidor, Izhar Bar-Gad, Yosef Yeshurun, Alon Korngreen. Mechanisms of Magnetic Stimulation of Central Nervous System Neurons. *PLoS Computational Biology* 7(3), March 2011.

BIBLIOGRAPHY

- [10] Robert Plonsey, Dennis B. Heppner. Considerations of Quasi-Stationarity in Electrophysiological Systems. *Bulletin of Mathematical Biophysics* 29, 1967.
- [11] A. Rotem and E. Moses. Magnetic Stimulation of Curved Nerves. *IEEE Transactions on Biomedical Engineering*. 53(3), 414-420, March 2006.
- [12] Bradley J. Roth, Peter J. Basser. A Model of the Stimulation of a Nerve Fiber by Electromagnetic Induction. *IEEE Transactions on Biomedical Engineering*. 37(6), June 1990.
- [13] Matthew N.O. Sadiku. *Elements of Electromagnetics*. Oxford University Press, New York, 2011
- [14] David Sterratt, Bruce Graham, Andre Gillies, David Willshaw. *Principles of Computational Modelling in Neuroscience*. Cambridge University Press, Cambridge, 2011.
- [15] P. S. Tofts. The Distribution of Induced Currents in Magnetic Stimulation of The Nervous System. *Phys. Med. Biol.* 35, 1119–1128, 1990.
- [16] Zsolt Turi, Claus Normann, Katharina Domschke, Andreas Vlachos. Transcranial Magnetic Stimulation in Psychiatry: Is There a Need for Electric Field Standardization? *Front. Hum. Neurosci.*. 15:639640. 2021. '<https://doi.org/10.3389/fnhum.2021.639640>'.
- [17] Tim Wagner, Jarrett Rushmore, Uri Eden, Antoni Valero-Cabre. Biophysical Foundations Underlying TMS: Setting The Stage for an Effective Use of Neurostimulation in The Cognitive Neurosciences. *Cortex* 45(9), October 2009.
- [18] Boshuo Wang, Warren M. Grill, and Angel V. Peterchev. Coupling Magnetically Induced Electric Fields to Neurons: Longitudinal and Transverse Activation. *Biophysical Journal* 115, 95–107, July 2018.
- [19] Alexis Wnuk, Alison Davis, Clinton Parks, Deborah Halber, Diane Kelly, Gail Zyla, Karen Hopkin, Karen Weintraub, Juliet M. Beverly, Knvul Safia Sheikh, Lindzi Wessel, Lisa Chiu, Marissa Fessenden, Melissa Galinato, Michael Richardson, Sandra Blumenrath, Susan Rojahn. *Brain Facts*. Society for Neuroscience, Washington, 2018.
- [20] Bruce Blaus. Blausen.com staff (2014). "Medical gallery of Blausen Medical 2014". *WikiJournal of Medicine*

- 1 (2). DOI:10.15347/wjm/2014.010. ISSN 2002-4436.
- Own work, CC BY 3.0, Downloaded 12.2022.
'<https://commons.wikimedia.org/w/index.php?curid=28761829>'.
- [21] Bruce Blaus. Blausen.com staff (2014). "Medical gallery of Blausen Medical 2014". *WikiJournal of Medicine* 1 (2). DOI:10.15347/wjm/2014.010. ISSN 2002-4436. - Derivative by Mikael Häggström, file: "Blausen_0211_CellMembrane.png", CC BY 3.0, Downloaded 12.2022. '<https://commons.wikimedia.org/w/index.php?curid=32538605>'.
- [22] Wikimedia Commons. Public Domain. Downloaded 12.2022. 'https://commons.wikimedia.org/wiki/File:Transcranial_magnetic_stimulation.jpg'



Norges miljø- og biovitenskapelige universitet
Noregs miljø- og biovitenskapelige universitet
Norwegian University of Life Sciences

Postboks 5003
NO-1432 Ås
Norway